J. Fluid Mech. (2011), *vol.* 669, *pp.* 260–297. © Cambridge University Press 2011
doi:10.1017/S002211201000501X

Multiscale tip asymptotics in hydraulic fracture with leak-off

DMITRY I. GARAGASH[1]†, EMMANUEL DETOURNAY[2] AND JOSE I. ADACHI[3]

[1]Dalhousie University, Department of Civil and Resource Engineering, 1360 Barrington Street, Halifax, Nova Scotia B3J 1Z1, Canada

[2]University of Minnesota, Department of Civil Engineering, 500 Pillsbury Drive, Minneapolis, MN 55455, USA, and CSIRO Earth Science and Resource Engineering, Technology Park, Kensington, WA 6151, Australia

[3]Schlumberger DCS, 1325 South Dairy Ashford Road, Houston, TX 77077, USA

(Received 27 April 2010; revised 22 September 2010; accepted 22 September 2010)

This paper is concerned with an analysis of the near-tip region of a fluid-driven fracture propagating in a permeable saturated rock. The analysis is carried out by considering the stationary problem of a semi-infinite fracture moving at constant speed V. Two basic dissipative processes are taken into account: fracturing of the rock and viscous flow in the fracture, and two fluid balance mechanisms are considered – leak-off and storage of the fracturing fluid in the fracture. It is shown that the solution is characterized by a multiscale singular behaviour at the tip, and that the nature of the dominant singularity depends both on the relative importance of the dissipative processes and on the scale of reference. This solution provides a framework to understand the interaction of representative physical processes near the fracture tip, as well as to track the changing nature of the dominant tip process(es) with the tip velocity and its impact on the global fracture response. Furthermore, it gives a universal scaling of the near-tip processes on the scale of the entire fracture and sets the foundation for developing efficient numerical algorithms relying on accurate modelling of the tip region.

Key words: boundary layer structure, magma and lava flow, porous media

1. Introduction

A particular class of fractures in the Earth develops as a result of internal pressurization by a viscous fluid. These fractures are either natural such as the kilometre-long volcanic dikes driven by magma coming from the upper mantle beneath the Earth's crust (Spence & Turcotte 1985; Emerman, Turcotte & Spence 1986) or man-made such as the hydraulic fractures created by injecting a viscous fluid from a borehole to increase production from oil or gas reservoirs (Economides & Nolte 2000) or to stimulate geothermal reservoirs (Mendelsohn 1984).

Since the pioneering work of Khristianovic & Zheltov (1955) and Barenblatt (1956), the construction of analytical and numerical solutions to the problem of a propagating hydraulic fracture has been the focus of numerous investigations.

† Email address for correspondence: garagash@dal.ca

https://doi.org/10.1017/S002211201000501X Published online by Cambridge University Press

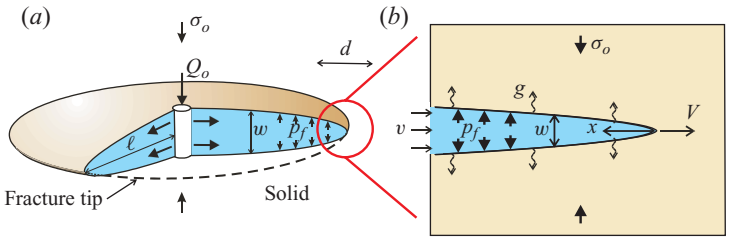


FIGURE 1. (Colour online) Sketch of a fluid-driven fracture (*a*) and its near-tip region modelled as a semi-infinite crack (*b*).

Progress has been slow, presumably because of the challenge of solving a problem characterized not only by a nonlinear system of integro-differential equations and a free boundary, but also by the existence of complex asymptotics at the propagating front of the fracture. Indeed, the construction of rigorous solutions, starting with papers by Spence & Sharp (1985), Spence, Sharp & Turcotte (1987) and Lister (1990) and continued with further recent contributions (Carbonell, Desroches & Detournay 1999; Savitski & Detournay 2002; Bunger, Detournay & Garagash 2005; Garagash & Detournay 2005; Garagash 2006*a*,*b*,*c*, 2010; Lecampion & Detournay 2007; Adachi & Detournay 2008; Peirce 2010), has hinged on explicitly using the relevant tip asymptote. Although restricted to particular cases, these solutions are not afflicted by the *ad hoc* simplifications of the first generation models (Perkins & Kern 1961; Geertsma & de Klerk 1969; Nordgren 1972; Abé, Mura & Keer 1976; Geertsma & Haafkens 1979; Advani *et al.* 1987). These efforts have led to the progressive recognition of the multiscale nature of the problem, with the formidable challenge it implies for constructing more general solutions using either analytical or numerical techniques.

Indeed, it is now understood that the non-locality, nonlinearity and history-dependence of the governing equations conspire to yield a complex solution structure that involves coupled processes at multiple small scales near the tip of the fracture. These near-tip processes and hierarchy of the corresponding scales, however, control the global response of fluid-driven fractures. For example, these new results imply that for a wide range of parameters, the classical square-root crack tip singularity of linear elastic fracture mechanics (LEFM) is not relevant at the typical scale of hydraulic fracturing treatments. Specifically, this happens when the energy expended in viscous fluid flow along the crack overshadows the energy required to overcome the resistance of the solid medium to an advancing crack tip. This resistance to crack propagation is embodied in the toughness of the solid material, which provides an upper limit to the strength of the LEFM singularity. Under these circumstances, the LEFM square-root singularity is localized in a thin boundary layer near the crack tip (Garagash & Detournay 2005), whereas the solution outside this layer is dominated by a different singularity that is associated with the flow of a viscous fluid in a narrowing elastic channel (Spence & Sharp 1985; Lister 1990; Desroches *et al.* 1994).

This paper deals with the near-tip region of a fluid-driven fracture propagating in a permeable rock mass: see figure 1. Specifically, we study the stationary problem of a semi-infinite fracture moving at constant speed V, under condition of plane strain. The analysis is carried out on the basis of the following assumptions: (i) the fracture propagates in accordance with LEFM (Rice 1968), (ii) the flow of an incompressible

https://doi.org/10.1017/S002211201000501X Published online by Cambridge University Press

viscous fluid in the crack is modelled by lubrication theory (Batchelor 1967) and (iii) the leak-off of fluid follows an 'inverse square root of time' behaviour (Carter 1957). Furthermore, we limit our considerations to cases where it can be assumed that the fluid front coincides with the fracture tip. This assumption is justified when the fluid lag is small compared with the relevant near-tip length scales of the fluid-driven fracture, which effectively imposes a lower bound limit to the far-field compressive stress σ_o perpendicular to the fracture (Garagash & Detournay 2000; Garagash 2009). Also, the zero-lag assumption implies that the fracture width and the net fluid pressure (the difference between the fluid pressure and σ_o) does not depend on σ_o.

This paper builds on previous research that deals with the problem of a steadily moving semi-infinite hydraulic fracture (Desroches *et al.* 1994; Lenoach 1995; Garagash & Detournay 2000). We will show that these previous results actually represent limiting cases of the general solution developed here.

2. Model formulation

2.1. *Problem definition*

The nature of the solution near the tip of a fluid-driven fracture can be investigated with the device of a semi-infinite plane strain fracture propagating at a constant velocity V, with the understanding that V represents the instantaneous local tip velocity of the parent fracture.

Before discussing the various assumptions behind the mathematical model, we introduce the moving coordinate x with origin at the crack tip, with $x > 0$ corresponding to the semi-infinite fracture (figure 1*b*). In the moving coordinate system x, the problem is stationary.

The semi-infinite fracture is assumed to propagate in a permeable linear elastic brittle medium, characterized by Young's modulus E and Poisson's ratio ν. The length scale associated with the dissipative processes taking place within the solid during rupture, e.g. the size of the process zone, is assumed to be small compared with the problem length scales that are yet to be defined, but which are themselves small compared with $\ell(t)$, the relevant characteristic length of the finite fracture. Linear elastic fracture mechanics is therefore used to model the quasi-static propagation of the fracture in the solid medium, which is thus further characterized by the toughness K_{Ic}.

The fracture is loaded externally by a far-field confining stress σ_o, and internally by a pressure $p_f(x)$ associated with the flow of an incompressible Newtonian fluid of viscosity μ; see figure 1(*b*). Fluid flow in the fracture is modelled under the usual assumptions of lubrication theory (Batchelor 1967). A negative singularity in fluid pressure typically develops if the fluid is allowed to reach the tip of the propagating fracture. This suggests the existence of a fluid lag zone, a cavity adjacent to the fracture tip, which is filled, in the case of an impermeable solid, by vapours of the fracturing fluid (Lister 1990; Rubin 1995), or, in the case of a permeable solid, by pore fluid circulating between the medium and the propagating fracture tip (Rubin 1993; Detournay & Garagash 2003). In our treatment of the problem, the fluid lag is neglected compared to the other problem length scales, on the assumption that σ_o is large enough, as discussed elsewhere (e.g. Garagash & Detournay 2000).

The exchange of fluid between the fracture and permeable host solid follows a simplified Carter law, where the local rate of fluid leak-off into the solid is proportional to the inverse square root of the 'exposure time', the time elapsed since the passing of the fracture front at that location; the coefficient of proportionality C_L is referred to as the Carter leak-off coefficient. Within the context of the stimulation of hydrocarbon

https://doi.org/10.1017/S002211201000501X Published online by Cambridge University Press

reservoirs, the applicability of the Carter law relies on the cake-building property of the industrial fracturing fluids (Economides & Nolte 2000).

2.2. *Governing equations*

The governing equations are expressed in terms of the crack opening $w(x)$, the average fluid velocity $v(x)$, and the fluid net pressure $p(x) = p_f(x) - \sigma_o$. They consist of a propagation criterion, an elasticity equation, and the lubrication equation. These equations make use of four material parameters,

$$E' = \frac{E}{1-\nu^2}, \quad K' = 4\left(\frac{2}{\pi}\right)^{1/2} K_{Ic}, \quad \mu' = 12\mu, \quad C' = 2C_L, \tag{2.1}$$

where E' is the plane strain modulus, and the alternate viscosity μ', toughness K' and the leak-off coefficient C' have been introduced to keep equations uncluttered by numerical factors.

2.2.1. *Fracture propagation*

The LEFM propagation criterion for a mode I fracture, $K_I = K_{Ic}$, is expressed here as an asymptotic condition on the crack opening w near the tip (Irwin 1957):

$$w = \frac{K'}{E'} x^{1/2}, \quad x \to 0. \tag{2.2}$$

2.2.2. *Elasticity equation*

The elastic relation between the net pressure $p(x)$ and the crack opening $w(x)$ is formulated as a singular integral equation (Bilby & Eshelby 1968):

$$p(x) = E' \mathscr{L}[w](x), \quad \text{with} \quad \mathscr{L}[w](x) = \frac{1}{4\pi} \int_0^\infty \frac{\mathrm{d}w}{\mathrm{d}s} \frac{\mathrm{d}s}{x-s}. \tag{2.3}$$

An inversion of (2.3), which accommodates the propagation condition (2.2), is (Garagash & Detournay 2000)

$$w = \frac{K'}{E'} x^{1/2} + \frac{1}{E'} \mathscr{L}^{-1}[p](x), \quad \text{with} \quad \mathscr{L}^{-1}[p](x) = \frac{4}{\pi} \int_0^\infty K(x,s)\, p(s)\, \mathrm{d}s, \tag{2.4}$$

where the integral kernel is defined as

$$K(x,s) = \ln \left| \frac{x^{1/2} + s^{1/2}}{x^{1/2} - s^{1/2}} \right| - 2\frac{x^{1/2}}{s^{1/2}}. \tag{2.5}$$

We point out that inversion (2.4)–(2.5) supports a wider class of solutions of (2.3) than the classical inversion (Rice 1968), which proves to be crucial for the solution of a semi-infinite fluid-driven fracture (Garagash & Detournay 2000).

2.2.3. *Fluid flow*

The stationary form of the local mass balance equation for an incompressible fluid in the moving coordinate system x is

$$V \frac{\mathrm{d}w}{\mathrm{d}x} - \frac{\mathrm{d}wv}{\mathrm{d}x} + g = 0, \tag{2.6}$$

where g is the leak-off rate, i.e. the local rate of flow out of the crack into the host permeable solid. The fluid velocity is related to the pressure gradient according to

https://doi.org/10.1017/S002211201000501X Published online by Cambridge University Press

Poiseuille's law (Batchelor 1967)

$$v = \frac{w^2}{\mu'}\frac{\mathrm{d}p}{\mathrm{d}x}, \tag{2.7}$$

while the leak-off rate is given by the Carter law (Carter 1957), namely that g is inversely proportional to the square root of the 'exposure time' at a fixed point:

$$g = C'\sqrt{\frac{V}{x}}. \tag{2.8}$$

The context around the Carter law is the build-up on the fracture walls of a filter cake, consisting of polymers and particulates, which is associated with leak-off of the fracturing fluid in the rock. This law derives mainly from assuming proportionality between the cake deposition rate and the leak-off rate, as well as a large contrast of permeability between the cake and the rock, with the consequence that the cake–rock interface can be approximated as a constant pore pressure boundary condition. Integrating the conservation equation (2.6) with the leak-off law (2.8) yields

$$v = V + C'V^{1/2}\frac{x^{1/2}}{w}. \tag{2.9}$$

(Both conditions of crack closure, $w_{|x=0} = 0$, and vanishing fluid flux, $(wv)_{|x=0} = 0$, at the tip have been applied in the integration.) It is worth noting that (2.9) implies that for zero leak-off ($C' = 0$), the fluid velocity v is equal to the fracture propagation velocity V everywhere along the crack (Desroches *et al.* 1994). In the general case ($C' < \infty$), (2.9) implies that $v = V$ represents the condition at infinity when $w \sim x^{\alpha}$ with $\alpha > 1/2$ as $x \to \infty$, while, as shown further, elasticity relation (2.3) further constrains the behaviour at infinity to $w \sim x^{2/3}$.

The set of equations consisting of the elasticity equation (2.3), Poiseuille's law (2.7), the fluid conservation equation (2.9) and the LEFM tip asymptote (2.2) governs the solution of a steadily propagating semi-infinite hydraulic fracture.

3. Asymptotics and structure of the general solution

3.1. *Vertex solutions*

The propagation regime of finite hydraulic fractures can advantageously be characterized by (i) the partitioning of the injected fluid volume between the crack and the host permeable solid (due to leak-off) and (ii) the partitioning of the total dissipated energy between the flow of the viscous fluid along the crack and the creation of new fracture surfaces at the tip. As the fracture grows with time, the partitioning of the fracturing fluid volume and of the dissipated energy evolves, leading to the emergence of limiting regimes over a certain range of time that is dominated by one storage mechanism and one dissipation mechanism. These concepts can be translated to the stationary problem of a semi-infinite hydraulic fracture, by recognizing that the partitioning of the injected fluid volume and of the dissipated energy depends on the distance from the crack tip rather than on time.

Before analysing the general case of the propagation of a semi-infinite hydraulic fracture, it is useful to consider limiting cases that are only characterized by one storage and one dissipation mechanism. Since the leak-off parameter C' is associated with fluid volume partitioning, while the fluid viscosity μ' and solid toughness K' affect the partitioning of the dissipated energy, four fundamental limiting regimes of fracture propagation exist: (i) storage–viscosity ($C' = 0$ and $K' = 0$),

https://doi.org/10.1017/S002211201000501X Published online by Cambridge University Press

Limiting solution	Opening $w(x)$	Net pressure $p(x)$	Velocity $v(x)$
(m) Storage–viscosity† $(C'=0,\ K'=0)$ (Desroches *et al.* 1994)	$\beta_0\,\ell_m^{1/3}\,x^{2/3}$	$\delta_0\,E'\,\dfrac{\ell_m^{1/3}}{x^{1/3}}$	V
$(\widetilde{m})$ Leak-off–viscosity† $(C'\to\infty,\ K'=0)$ (Lenoach 1995)	$\tilde{\beta}_0\,\ell_{\tilde{m}}^{3/8}\,x^{5/8}$	$\tilde{\delta}_0\,E'\,\dfrac{\ell_{\tilde{m}}^{3/8}}{x^{3/8}}$	$\dfrac{V}{\tilde{\beta}_0}\,\dfrac{\ell_{\tilde{m}}^{9/8}}{\ell_m\,x^{1/8}}$
(k) Toughness $(\mu'=0)$	$\ell_k^{1/2}\,x^{1/2}$	0	$V+\chi\,V$

†Coefficients: $\beta_0=2^{1/3}3^{5/6}$, $\delta_0=\beta_0\,f(2/3)$, $\tilde{\beta}_0=4/(15^{1/4}\,(\sqrt{2}-1)^{1/4})$, $\tilde{\delta}_0=\tilde{\beta}_0\,f(5/8)$.

TABLE 1. Three fundamental limiting solutions of a semi-infinite hydraulic fracture without lag, defined in terms of the length scales (3.3) and number χ (3.4).

(ii) leak-off–viscosity ($C'\to\infty$ and $K'=0$), (iii) storage–toughness ($C'=0$ and $\mu'=0$), and (iv) leak-off–toughness ($C'\to\infty$ and $\mu'=0$). (The term 'storage' refers to storage of fluid in the crack as opposed to the fluid leak-off into the host pervious solid.)

These four limiting solutions are known and belong to the class of exact solutions of the elasticity equation (2.3) (e.g. Kanninen & Popelar 1985):

$$w_\lambda(x)=B\,x^\lambda,\quad p_\lambda(x)=E'\,B\ f(\lambda)\,x^{\lambda-1},\quad \text{with}\quad f(\lambda)=\frac{\lambda\cot\pi\lambda}{4}\quad\text{and}\quad 0<\lambda<1, \tag{3.1}$$

where B is an arbitrary constant. Specific values of the exponent λ and the coefficient B for the four solutions of interest can be obtained by substitution of (3.1) into the lubrication equation

$$\frac{w^2}{\mu'}\frac{\mathrm{d}p}{\mathrm{d}x}=v=V+C'V^{1/2}\,\frac{x^{1/2}}{w} \tag{3.2}$$

obtained by combining Poiseuille's law (2.7) and the fluid balance law (2.9), and setting the appropriate pair of material parameters to the limiting values identified above. In the toughness-dominated case ($\mu'=0$), $\lambda=1/2$ according to the fracture propagation condition (2.2) and the corresponding net pressure is thus null in view of (3.1). Although Poiseuille's law becomes meaningless when $\mu'=0$ (and thus the first equality in (3.2) becomes indeterminate), the expression for the fluid velocity in this case is recovered from the fluid balance, the second equality in (3.2), as $v=V+C'V^{1/2}E'/K'$. Also, in the leak-off-dominated solutions ($C'\to\infty$), the first term on the right-hand side of (3.2) is negligible compared with the second term.

The resulting solutions are summarized in table 1. In the context of the general solution, these particular cases are referred to as vertex solutions, with the m-vertex corresponding to the storage–viscosity case ($C'=0$ and $K'=0$), the $\widetilde{m}$-vertex for the leak-off–viscosity case ($C'\to\infty$ and $K'=0$), and the k-vertex for both the storage–toughness ($C'=0$ and $\mu'=0$) and leak-off–toughness regimes ($C'\to\infty$ and $\mu'=0$). The m-vertex is actually the particular case considered by Desroches *et al.* (1994), while the $\widetilde{m}$-vertex is the solution obtained by Lenoach (1995). The vertex solutions listed in table 1 are expressed in terms of three length scales,

$$\ell_k=\left(\frac{K'}{E'}\right)^2,\quad \ell_m=V\frac{\mu'}{E'},\quad \ell_{\tilde{m}}=\left(C'V^{1/2}\frac{\mu'}{E'}\right)^{2/3}, \tag{3.3}$$

https://doi.org/10.1017/S002211201000501X Published online by Cambridge University Press

and a number χ defined as

$$\chi = \frac{\ell_{\tilde{m}}^{3/2}}{\ell_m \ell_k^{1/2}} = \frac{C'E'}{V^{1/2}K'}. \tag{3.4}$$

This number permits discrimination between the two limits ($C'=0$ and $C'\to\infty$) associated with the k-vertex ($\mu'=0$) by setting $\chi=0$ and $\chi\to\infty$, respectively. The three length scales defined in (3.3) have been introduced for convenience but they do not have, in view of the self-similar nature of the vertex solutions, any particular meaning other than the distance from the tip at which the fracture opening at any of the vertices is of the same order as the corresponding length scale (e.g. at the m-vertex, $w(x)\sim\ell_m$ when $x\sim\ell_m$).

3.2. *Edge solutions*

The vertex similarity solutions summarized in table 1 actually have a broader meaning, as they can also be regarded as asymptotics of the general solution of the system of (2.2), (2.3), (2.7) and (2.9). (The proof of this conjecture for a general monomial form (3.1) as the near or far-field asymptote of elasticity equation (2.3) is given in Appendix A.) Indeed, consider the general case when the three length scales (3.3) are non-zero and bounded. Comparing the power laws for the opening in the similarity solutions (2/3, 5/8 and 1/2 for the m-, $\widetilde{m}$- and k-vertices, respectively), it is evident that the toughness k-asymptote dominates the near field ($x\to 0$) while the storage–viscosity m-asymptote prevails in the far field ($x\to\infty$). In the special cases when either ℓ_k or ℓ_m vanishes (or, alternatively, when $\ell_{\tilde{m}}$ is large), the leak-off–viscosity $\widetilde{m}$-asymptote has to emerge in the near field of the viscosity-dominated solution or in the far field of the toughness-dominated solution, respectively.

The general solution of a semi-infinite fracture therefore establishes the transition between the far-field m- and the near-field k-asymptotes, with the $\widetilde{m}$-asymptote emerging in the intermediate field if the effect of either storage or toughness on the solution is small enough or if the effect of leak-off is large enough. To gain further insight into the solution structure, we now consider three particular 'edge' solutions, each corresponding to a specific situation in which one of the three length scales ℓ_k, ℓ_m or $\ell_{\tilde{m}}$ is exactly zero while the other two are non-zero and bounded.

(i) In the zero-leak-off case ($\ell_{\tilde{m}}=0$), the resulting storage mk-solution corresponds to the transition from the far-field m- to the near-field k-asymptotes. The length scale characterizing the transition region can be estimated by requiring that the near- and far-field asymptotes, when formally extended into this region, are comparable, i.e. $w\sim\ell_k^{1/2}x^{1/2}\sim\ell_m^{1/3}x^{2/3}$. Thus, the transition occurs at distances $x\sim\ell_{mk}=\ell_k^3/\ell_m^2$ from the tip, which places the near- and far-field asymptotic regions at $x\ll\ell_{mk}$ and $x\gg\ell_{mk}$, respectively.

(ii) In the zero-toughness case ($\ell_k=0$), the resulting viscosity $m\widetilde{m}$-solution corresponds to the transition from the far-field m- to the near-field $\widetilde{m}$-asymptotes at distances $x\sim\ell_{m\tilde{m}}=\ell_{\tilde{m}}^9/\ell_m^8$ from the tip.

(iii) In the zero-storage case ($\ell_m\to 0$ or $\ell_{\tilde{m}}\to\infty$), the resulting leak-off $\widetilde{m}k$-solution corresponds to the transition from the far-field $\widetilde{m}$- to the near-field k-asymptotes at distances $x\sim\ell_{\tilde{m}k}=\ell_k^4/\ell_{\tilde{m}}^3$ from the tip.

A solution characterized by a small but non-zero toughness and storage is a perturbation of both the viscosity $m\widetilde{m}$- and the leak-off $\widetilde{m}k$-edge solutions. It is to be expected then that the perturbed solution is approximated by both edge solutions but over different parts of the semi-infinite crack. This is accomplished if there exists an intermediate range of distances from the crack tip where the two

https://doi.org/10.1017/S002211201000501X Published online by Cambridge University Press

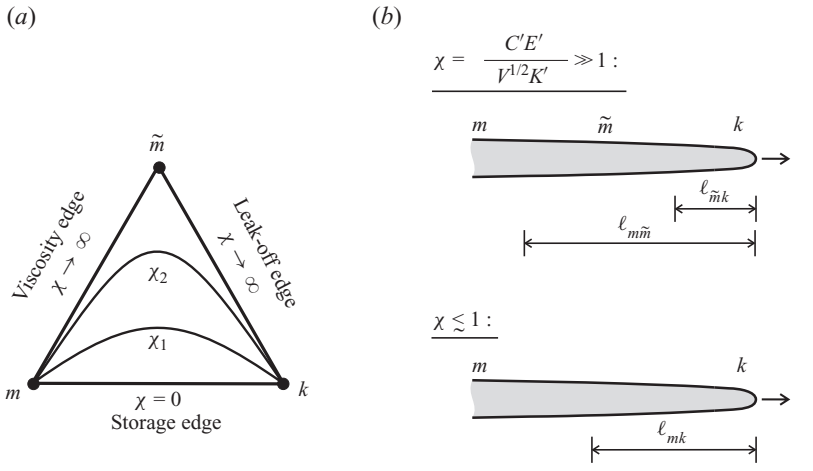


FIGURE 2. (*a*) Parametric diagram and few solution 'trajectories' parametrized by number χ; (*b*) schematic structure of the solutions for $\chi \lesssim 1$ and $\chi \gg 1$.

limiting solutions match, i.e. possess the common $\tilde{m}$-asymptote. Recalling that the $\tilde{m}$-asymptote is realized at distances $x \ll \ell_{m\tilde{m}}$ and $x \gg \ell_{\tilde{m}k}$ from the tip in the viscosity- and leak-off-dominated solutions, respectively, the matching of the two solutions (in the framework of a perturbed solution) requires separation of the two transition length scales, i.e. $\ell_{m\tilde{m}} \gg \ell_{\tilde{m}k}$.

To cast the above discussion in terms of the trajectory number χ defined in (3.4), the storage mk-solution corresponds to $\chi = 0$, while both viscosity $m\tilde{m}$ and leak-off $\tilde{m}k$ solutions correspond to $\chi \to \infty$. Furthermore, noting the alternative representations of χ in terms of the transition length scales

$$\chi = \left(\frac{\ell_{m\tilde{m}}}{\ell_{mk}}\right)^{1/6} = \left(\frac{\ell_{m\tilde{m}}}{\ell_{\tilde{m}k}}\right)^{1/8} = \left(\frac{\ell_{mk}}{\ell_{\tilde{m}k}}\right)^{1/2}, \tag{3.5}$$

the condition $\ell_{m\tilde{m}} \gg \ell_{\tilde{m}k}$ is in fact equivalent to $\chi^8 \gg 1$. Under these conditions, the solution can be approximated by the $m\tilde{m}$ and $\tilde{m}k$ solutions matched over the intermediate $\tilde{m}$-asymptote.

3.3. *Structure of solution*

The solution structure is schematically shown on the triangular parametric diagram in figure 2, with the vertices m, $\tilde{m}$ and k corresponding to the three fundamental solutions from table 1. The solution trajectory, parametrized by the number χ (3.4)–(3.5) is a conceptual representation of the changing nature of the solution with distance from the tip. By emerging from the k-vertex and ending at the m-vertex, the solution trajectory indicates how the solution evolves from the toughness asymptote (the k-vertex) as $x \to 0$ to the storage–viscosity asymptote (the m-vertex) as $x \to \infty$ (figure 2*a*). When $\chi = 0$, the solution trajectory spans the storage mk-edge along which the transition between the near- and far-field asymptotes takes place over the length scale ℓ_{mk} (figure 2*b*). With increasing $\chi > 0$, the trajectory is pulled towards the leak-off–viscosity $\tilde{m}$-vertex. When $\chi \gg 1$ ($\ell_{m\tilde{m}} \gg \ell_{mk} \gg \ell_{\tilde{m}k}$), the trajectory essentially spans first the leak-off $\tilde{m}k$-edge, and then the $m\tilde{m}$-edge, thus providing a transition between the k-vertex and the m-vertex, via the $\tilde{m}$-vertex (figure 2*b*).

These considerations allow us to describe the changing nature of the tip solution with the crack tip velocity V. According to expression (3.4) for the trajectory number

https://doi.org/10.1017/S002211201000501X Published online by Cambridge University Press

χ, we have

$$\chi \propto V^{-1/2}. \tag{3.6}$$

With decreasing V, a solution trajectory in the parametric space $m\widetilde{m}k$ (figure 2a) is thus pulled away from the storage mk-edge towards the leak-off $\widetilde{m}k$-edge. This change in the solution trajectory signifies the increasing influence of the leak-off on the solution and the emergence of the leak-off–viscosity $\widetilde{m}$-asymptote at intermediate distances from the crack tip. Furthermore, according to the expressions (3.3) for the transition length scales ℓ_{mk}, $\ell_{\widetilde{m}k}$ and $\ell_{m\widetilde{m}}$

$$\ell_{mk} \propto V^{-2}, \qquad \ell_{m\widetilde{m}} \propto V^{-5}, \qquad \ell_{\widetilde{m}k} \propto V^{-1}. \tag{3.7}$$

The increase in the transition length scales with decreasing crack tip velocity V implies a shrinking range of distances from the tip, $x \gg \max\{\ell_{mk}, \ell_{m\widetilde{m}}\}$, which is dominated by the m-asymptote and an expanding range of distances from the tip dominated either by the $\widetilde{m}$-asymptote, $\ell_{m\widetilde{m}} \gg x \gg \ell_{\widetilde{m}k}$, or by the k-asymptote, $x \ll \min\{\ell_{mk}, \ell_{\widetilde{m}k}\}$ (figure 2b). Since the tip velocity of a finite fracture decreases with time (at least under a constant injection rate), the tip solution interpreted from this stationary solution is seen to evolve with time. In other words, as the length scales ℓ_{mk}, $\ell_{\widetilde{m}k}$ and $\ell_{m\widetilde{m}}$ evolve with time, the nature of the solution in the tip region at a given physical scale changes accordingly.

3.4. *Asymptotic expansions of the vertices*

Further insight into the solution can be gained by constructing asymptotic expansions near the vertices of the parametric space of figure 2(a), building on procedures introduced by Garagash & Detournay (2005) in their treatment of the zero leak-off case (mk-solution).

3.4.1. *Near-field k-expansion*

The near-field k-asymptote does not depend on the fluid viscosity μ'. The departure of the solution from the k-asymptote with distance from the tip corresponds to an increasing influence of viscosity, and can be quantified by considering the following k-asymptotic expansion (see Appendix B):

$$\begin{aligned} x \to 0: \quad w &= \ell_k^{1/2} x^{1/2} \left[1 + 4\pi \frac{x^{1/2}}{\ell_1^{1/2}} + 64 \frac{x \ln x}{(\ell_1\, \ell_2)^{1/2}} \right] \\ \frac{p}{E'} &= \frac{\ell_k^{1/2}}{\ell_1^{1/2}} \Bigg[0 + \ln\left(\frac{x}{x^o(\chi)}\right) - 24\pi \frac{x^{1/2}}{\ell_2^{1/2}} - 192 \frac{x \ln x}{\ell_2} \Bigg]. \end{aligned} \tag{3.8}$$

viscosity corrections

The length scales ℓ_1 and ℓ_2, defined in terms of ℓ_{mk} and $\ell_{\widetilde{m}k}$ as

$$\ell_1 = \left(\ell_{mk}^{-1/2} + \ell_{\widetilde{m}k}^{-1/2}\right)^{-2}, \qquad \ell_2 = \left(\tfrac{2}{3}\ell_{mk}^{-1/2} + \ell_{\widetilde{m}k}^{-1/2}\right)^{-2}, \tag{3.9}$$

underpin the dependence on μ' of the next-order correction terms in the expansion (3.8). Since $\ell_{mk} = \chi^2\, \ell_{\widetilde{m}k}$, both ℓ_1 and ℓ_2 reduce, up to an $O(1)$ factor, to either ℓ_{mk} or $\ell_{\widetilde{m}k}$ under storage ($\chi \to 0$) or leak-off ($\chi \to \infty$) dominated conditions, respectively. The expansion for fluid velocity v is omitted in (3.8) and in the following treatment of asymptotic expansions, as it can be readily written out by substituting the corresponding opening expansion into the lubrication equation and expanding for small or large x. All the coefficients in the k-expansion are known from the asymptotic analysis, except for the uniform pressure term proportional to $\ln x^o$ that results from

https://doi.org/10.1017/S002211201000501X Published online by Cambridge University Press

integrating the lubrication equation. This term can be only found as a part of the numerical solution over the complete range of distances from the tip (and not from the near-field asymptotic analysis alone).

3.4.2. *Far-field m-expansion*

The far-field m-asymptote is independent of the toughness K' and the leak-off coefficient C'. The departure of the solution from the m-vertex when moving towards the tip is quantified by an asymptotic expansion, where the effects of toughness and leak-off are embodied in the next-order correction terms of the monomial form (3.1). These corrections are obtained by balancing asymptotic terms in the lubrication equation for large x (see Appendix C for details). The resulting far-field asymptotic expansion is

$$x \to \infty : \quad w = \ell_m^{1/3}\, x^{2/3} \left[\beta_0 + \underbrace{\sum_{j=1}^{3} \beta_{-j} \left(\frac{\ell_{m\tilde{m}}}{x} \right)^{j/6}}_{} + \underline{\underline{(\beta_{-4})_*(\chi) \left(\frac{\ell_{m*}}{x} \right)^{2/3-h}}} \right],$$

$$\frac{p}{E'} = \ell_m^{1/3} x^{-1/3} \left[\delta_0 + \underbrace{\sum_{j=1}^{3} \delta_{-j} \left(\frac{\ell_{m\tilde{m}}}{x} \right)^{j/6}}_{\text{leak-off corrections}} + \underbrace{\underline{\underline{(\delta_{-4})_*(\chi) \left(\frac{\ell_{m*}}{x} \right)^{2/3-h}}}}_{\text{toughness/leak-off corrections}} \right], \tag{3.10a, b}$$

where $h \simeq 0.1387$ and the known expansion coefficients are given by

$$\beta_0 = 2^{1/3} 3^{5/6}, \quad \beta_{-1} = \frac{1}{2}, \quad \beta_{-2} = -\frac{3^{1/6}}{2^{7/3}}, \quad \beta_{-3} = \frac{2^{7/3}}{3^{5/3}}, \tag{3.11}$$

and by $\delta_{-j} = \beta_{-j}\, f\,(2/3 - j/6)$ for $j = 0, 1, 2, 3$; and $(\delta_{-4})_* = (\beta_{-4})_*\, f\,(h)$ with function f defined in (3.1).

The first three next-order terms (under the sum sign) in (3.10a) are scaled by $\ell_{m\tilde{m}}$, and therefore correspond to the leak-off corrections to the storage–viscosity m-asymptote. In the last expansion term, either $\ell_{m\tilde{m}}$ or ℓ_{mk} are appropriate since the corresponding coefficient, either $(\beta_{-4})_{\tilde{m}}$ or $(\beta_{-4})_k$, cannot be obtained from asymptotic considerations only, and is therefore a part of the complete numerical solution. This term embodies the effects of both toughness and leak-off onto the far field. Given the relation of the transition length scales to χ (3.5), the coefficients $(\beta_{-4})_{\tilde{m}}$ or $(\beta_{-4})_k$ in (3.10a) are related by

$$(\beta_{-4})_k(\chi) = \chi^{4-6h}\, (\beta_{-4})_{\tilde{m}}(\chi). \tag{3.12}$$

3.4.3. *Intermediate-field $\tilde{m}$-expansion ($\chi \gg 1$)*

Under the condition $\chi \gg 1$, the intermediate-field $\tilde{m}$-asymptote emerges at distances $\ell_{m\tilde{m}} \gg x \gg \ell_{\tilde{m}k}$ from the crack tip. The departure of the solution from the $\tilde{m}$-asymptote with decreasing (increasing) distance from the tip corresponds to an increasing effect of toughness (storage) on the solution, and can be viewed on the parametric diagram (figure 2a) as a perturbation of the corresponding $\tilde{m}$-vertex along the leak-off $\tilde{m}k$-edge (viscosity $\tilde{m}m$-edge). The corresponding asymptotic expansion is given by

https://doi.org/10.1017/S002211201000501X Published online by Cambridge University Press

(see Appendix D)

$\ell_{\widetilde{m}k} \ll x \ll \ell_{m\widetilde{m}}$:

$$w = \ell_{\widetilde{m}}^{3/8} x^{5/8} \left[\underline{\tilde{\beta}_{-1} \left(\frac{\ell_{\widetilde{m}k}}{x} \right)^{5/8-\tilde{h}}} + \tilde{\beta}_0 + \underline{\underline{\sum_{j=1}^{3} \tilde{\beta}_j \left(\frac{x}{\ell_{m\widetilde{m}}} \right)^{j/8}}} \right],$$

$$\frac{p}{E'} = \ell_{\widetilde{m}}^{3/8} x^{-3/8} \left[\underbrace{\tilde{\delta}_{-1} \left(\frac{\ell_{\widetilde{m}k}}{x} \right)^{5/8-\tilde{h}}}_{\text{toughness correction}} + \tilde{\delta}_0 + \underbrace{\underline{\underline{\sum_{j=1}^{2} \tilde{\delta}_j \left(\frac{x}{\ell_{m\widetilde{m}}} \right)^{j/8}} + \tilde{\delta}_3 \left(\frac{x}{\ell_{m\widetilde{m}}} \right)^{3/8} \ln \left(\frac{x}{\tilde{x}^o} \right)}}_{\text{storage corrections}} \right], \tag{3.13a, b}$$

where $\tilde{h} \approx 0.06999$, and the known expansion coefficients are given by

$$\tilde{\beta}_0 \approx 2.53356, \quad \tilde{\beta}_1 \approx 1.30165, \quad \tilde{\beta}_2 \approx -0.451609, \quad \tilde{\beta}_3 \approx 0.183355 \tag{3.14}$$

and by $\tilde{\delta}_{-1} = \tilde{\beta}_{-1}\, f(\tilde{h})$; $\tilde{\delta}_j = \tilde{\beta}_j\ f\,(5/8 + j/8)$ for $j = 0, 1, 2$; and $\tilde{\delta}_3 = (1/4\pi)\tilde{\beta}_3$.

The two groups of terms identified in (3.13a, b) correspond to the toughness and storage corrections to the leading leak-off–viscosity-dominated $\widetilde{m}$-asymptote in the intermediate range of distances from the tip. In the zero-storage limit $\ell_{m\widetilde{m}} = \infty$, the leading term and the toughness correction form the far-field expansion ($\ell_{\widetilde{m}k} \ll x < \infty$) of the $\widetilde{m}k$-edge solution (see Appendix D.1). In the zero-toughness limit $\ell_{\widetilde{m}k} = 0$, the leading term and the storage corrections give the near-field expansion ($0 < x \ll \ell_{m\widetilde{m}}$) of the $m\widetilde{m}$-edge solution (see Appendix D.2). For large (but bounded) χ (i.e. $0 < \ell_{\widetilde{m}k} \ll \ell_{m\widetilde{m}} < \infty$), these two limit-case expansions can be combined to form the general $\widetilde{m}$-expansion (3.13a, b), valid at intermediate distances from the tip. Indeed, it is shown in Appendix D.3 that (3.13a, b) gives an identical form of the perturbations of the $\widetilde{m}k$-edge and the $m\widetilde{m}$-edge solutions in the small parameter $\chi^{-1} = (\ell_{\widetilde{m}k}/\ell_{m\widetilde{m}})^{1/8}$ in the common intermediate range of distances from the tip. These perturbed edge solutions (although not explicitly constructed) can therefore be matched over the common intermediate $\widetilde{m}$-expansion to provide the next-order large χ solution for a semi-infinite fluid-driven fracture.

As in the case of the coefficient in the last term in the m-expansion (3.10a, b), the coefficient $\tilde{\beta}_{-1}$ in the toughness correction term in (3.13a) is undetermined by the asymptotic analysis and is a part of the numerical $\widetilde{m}k$-edge solution. Moreover, the parameter $\tilde{x}^o$ in the last storage correction term in (3.13b) is not constrained by the asymptotic considerations either, and is later recovered from the numerical $m\widetilde{m}$-edge solution.

4. Scaling

The definition of a scaling for this problem entails introducing the following characteristic quantities: a distance from the tip ℓ_*, a width w_*, a pressure p_* and a fluid velocity v_*. These quantities enable us to define in turn the normalized coordinate ξ and the normalized field variables, namely the crack opening $\Omega(\xi)$, the net pressure $\Pi(\xi)$ and the fluid velocity $\vartheta(\xi)$ as

$$\xi = x/\ell_*, \quad \Omega = w/w_*, \quad \Pi = p/p_*, \quad \vartheta = v/v_*. \tag{4.1}$$

Three distinct scaling schemes of the form (4.1) can be defined to study the transition solution between (i) the far field (m-vertex) and the near field (k-vertex); and, in the case $\chi \gg 1$, (ii) the far field (m-vertex) and the intermediate field ($\widetilde{m}$-vertex);

https://doi.org/10.1017/S002211201000501X Published online by Cambridge University Press

Scaling	ℓ_*	w_*	p_*	v_*
mk	$\ell_{mk} = \ell_k^3/\ell_m^2$	ℓ_k^2/ℓ_m	$E'\,\ell_m/\ell_k$	V
$m\widetilde{m}$	$\ell_{m\widetilde{m}} = \ell_{\widetilde{m}}^9/\ell_m^8$	$\ell_{\widetilde{m}}^6/\ell_m^5$	$E'\,(\ell_m/\ell_{\widetilde{m}})^3$	V
$\widetilde{m}k$	$\ell_{\widetilde{m}k} = \ell_k^4/\ell_{\widetilde{m}}^3$	$\ell_k^{5/2}/\ell_{\widetilde{m}}^{3/2}$	$E'\,(\ell_{\widetilde{m}}/\ell_k)^{3/2}$	$\chi\,V$

TABLE 2. Characteristic distance from the tip ℓ_*, width w_*, pressure p_* and fluid velocity v_* corresponding to the three scalings (4.1) of the problem.

Scaling	Lubrication (3.2) $\vartheta(\xi) =$	Elasticity (2.3)	Propagation (2.2) $\xi \to 0$
mk	$\Omega^2\,(\mathrm{d}\Pi/\mathrm{d}\xi) = 1 + \chi\,\xi^{1/2}/\Omega$		$\Omega = \xi^{1/2}$
$m\widetilde{m}$	$\Omega^2\,(\mathrm{d}\Pi/\mathrm{d}\xi) = 1 + \xi^{1/2}/\Omega$	$\Pi = \mathscr{L}[\Omega](\xi)$	$\Omega = \chi^{-1}\,\xi^{1/2}$
$\widetilde{m}k$	$\Omega^2\,(\mathrm{d}\Pi/\mathrm{d}\xi) = \chi^{-1} + \xi^{1/2}/\Omega$		$\Omega = \xi^{1/2}$

TABLE 3. Normalized governing equations in different scalings.

and (iii) the intermediate field ($\widetilde{m}$-vertex) and the near field (k-vertex), by setting the length scale ℓ_* equal to the corresponding transition length scales ℓ_{mk}, $\ell_{m\widetilde{m}}$ and $\ell_{\widetilde{m}k}$, respectively. The remaining characteristic quantities (i.e. w_*, v_*, p_*) for each scaling follow from the evaluation of either of the two corresponding asymptotic solutions at $x = \ell_*$. For example, the scaling corresponding to the mk-edge solution is given by $\ell_* = \ell_{mk}$, $w_* = \ell_m^{1/3}\ell_*^{2/3} = \ell_k^{1/2}\ell_*^{1/2}$, $v_* = V$ and $p_* = E'\,\ell_m^{1/3}/\ell_*^{1/3}$. (Note that the $O(1)$ numerical coefficients resulting from evaluating, in this case, the far-field asymptote at $x = \ell_*$ were dropped in the resulting expressions for w_* and p_*.)

The sets of characteristic quantities for the three scaling schemes are summarized in table 2 in terms of the primary length scales (3.3) and the dimensionless number χ (3.4). The relations between these three scalings depend only on χ as

$$\xi_{mk} = \chi^6\,\xi_{m\widetilde{m}} = \chi^{-2}\,\xi_{\widetilde{m}k}, \quad \Omega_{mk} = \chi^4\,\Omega_{m\widetilde{m}} = \chi^{-1}\,\Omega_{\widetilde{m}k}, \quad \Pi_{mk} = \chi^{-2}\,\Pi_{m\widetilde{m}} = \chi\,\Pi_{\widetilde{m}k},$$
$$\vartheta_{mk} = \vartheta_{m\widetilde{m}} = \chi\,\vartheta_{\widetilde{m}k}, \tag{4.2}$$

where the indices were added to identify the respective scalings as in table 2.

The governing equations in the three scalings are given in table 3. As expected, the equations are parametrized by the same unique number χ in any scaling, since χ carries the meaning of a leak-off parameter in the storage mk-scaling, while χ^{-1} can be interpreted as toughness in the viscosity $m\widetilde{m}$-scaling and as storage in the leak-off $\widetilde{m}k$-scaling.

Normalized expressions for the near (3.8), far (3.10a, b) and intermediate (3.13a, b) asymptotic expansions are presented in Appendix E for further reference.

5. Solution

5.1. *Approach*

Using the general structure of the solution shown in figure 2 as a road map, we now seek to compute the solution in the region between the near field, $x \ll \min\{\ell_{mk}, \ell_{\widetilde{m}k}\}$, and the far field, $x \gg \max\{\ell_{mk}, \ell_{m\widetilde{m}}\}$. The solution can be constructed in either of

https://doi.org/10.1017/S002211201000501X Published online by Cambridge University Press

the scalings given by (4.1) and table 2, by solving the corresponding set of equations from table 3 for an arbitrary value of the trajectory number $\chi \in [0, \infty)$. Since $\chi = 0$ corresponds to the mk-edge of the parametric $m\widetilde{m}k$-space (figure 2*a*), we use the mk-scaling to compute the solution for a finite χ. In the limiting case $\chi \to \infty$, the other two ($m\widetilde{m}$ and $\widetilde{m}k$) scalings have to be used to capture the corresponding two parts of the composite solution: the $m\widetilde{m}$-solution away from the tip and the $\widetilde{m}k$-solution near the tip (figure 2*b*).

The numerical solution is sought over an interval $x \in (X_0, X_\infty)$, which embeds the transition region between the k- and m-asymptotes (table 1). In the limit $\chi \to \infty$, two intervals, $x \in (X_0, \widetilde{X}_\infty)$ and $x \in (\widetilde{X}_0, X_\infty)$, are used to compute the $\widetilde{m}k$-edge and $m\widetilde{m}$-edge solutions, respectively. The bounds of these computational intervals are to be rooted in the respective asymptotic fields. The use of asymptotic expansions in the near, far and intermediate fields allows us to reduce the intervals where the solution is computed.

The numerical method entails a discretization of the computational interval into a certain number of elements and relies on assuming a piecewise smooth approximation of the net pressure over that interval and on evaluating exactly the corresponding opening from the elasticity integral. Then, the opening and pressure approximations are substituted into a finite-volume approximation of the lubrication equation, which is eventually solved for the pressure at the discretization nodes; see Appendix F for details of the numerical method.

5.2. *Edge solutions*

The net pressure Π and the crack opening Ω for the three edges of the $m\widetilde{m}k$-space are shown in figure 3 in their respective scalings. The asymptotic expansions presented in § 3.4 (shown by dashed lines) continue these solutions outside the computational intervals. The leading terms in these expansions (the k, m and $\widetilde{m}$ asymptotes) are shown by dotted lines with a log-log slope.

Specifically, the near-field expansions of the mk- and $\widetilde{m}k$-edge solutions are given by the k-expansion (3.8) in the limits $\chi \to 0$ and $\chi \to \infty$, respectively. The corresponding values of the expansion coefficient x^o obtained from these edge solutions are

$$x^o(0) \simeq 4.07\ 10^{-3}\, \ell_{mk}, \qquad x^o(\infty) \simeq 1.5\ 10^{-3}\, \ell_{\widetilde{m}k}. \tag{5.1}$$

The far-field expansions of the mk- and $m\widetilde{m}$-edge solutions are given by the respective limits of the m-expansion (3.10*a*, *b*). The corresponding values of the *a priori* unknown expansion coefficient β_{4*} are

$$(\beta_{-4})_k\,(0) \simeq 0.0372, \qquad (\beta_{-4})_{\widetilde{m}}\,(\infty) \simeq -0.7406. \tag{5.2}$$

Finally, the expansions in the near field of the $m\widetilde{m}$-edge solution and in the far field of the $\widetilde{m}k$-edge solution are given by the reductions of the intermediate $\widetilde{m}$-expansion (3.13*a*, *b*) when $\ell_{\widetilde{m}k} = 0$ and $\ell_{m\widetilde{m}} = \infty$, respectively. The numerical values of the coefficients in these expansions that cannot be determined by asymptotic analysis are

$$\tilde{x}^o \simeq 1.124\, \ell_{m\widetilde{m}}, \qquad \tilde{\beta}_{-1} \simeq 0.0161. \tag{5.3}$$

5.3. *General numerical solution*

Figures 4–6 illustrate the numerical solution computed in the mk-scaling. Plots of the net pressure and opening shown in figure 4 for three values of χ describe the departure of the solution from the storage-dominated limit (mk-edge, $\chi = 0$), and the early stages of development of the intermediate leak-off-dominated field. Departure

https://doi.org/10.1017/S002211201000501X Published online by Cambridge University Press

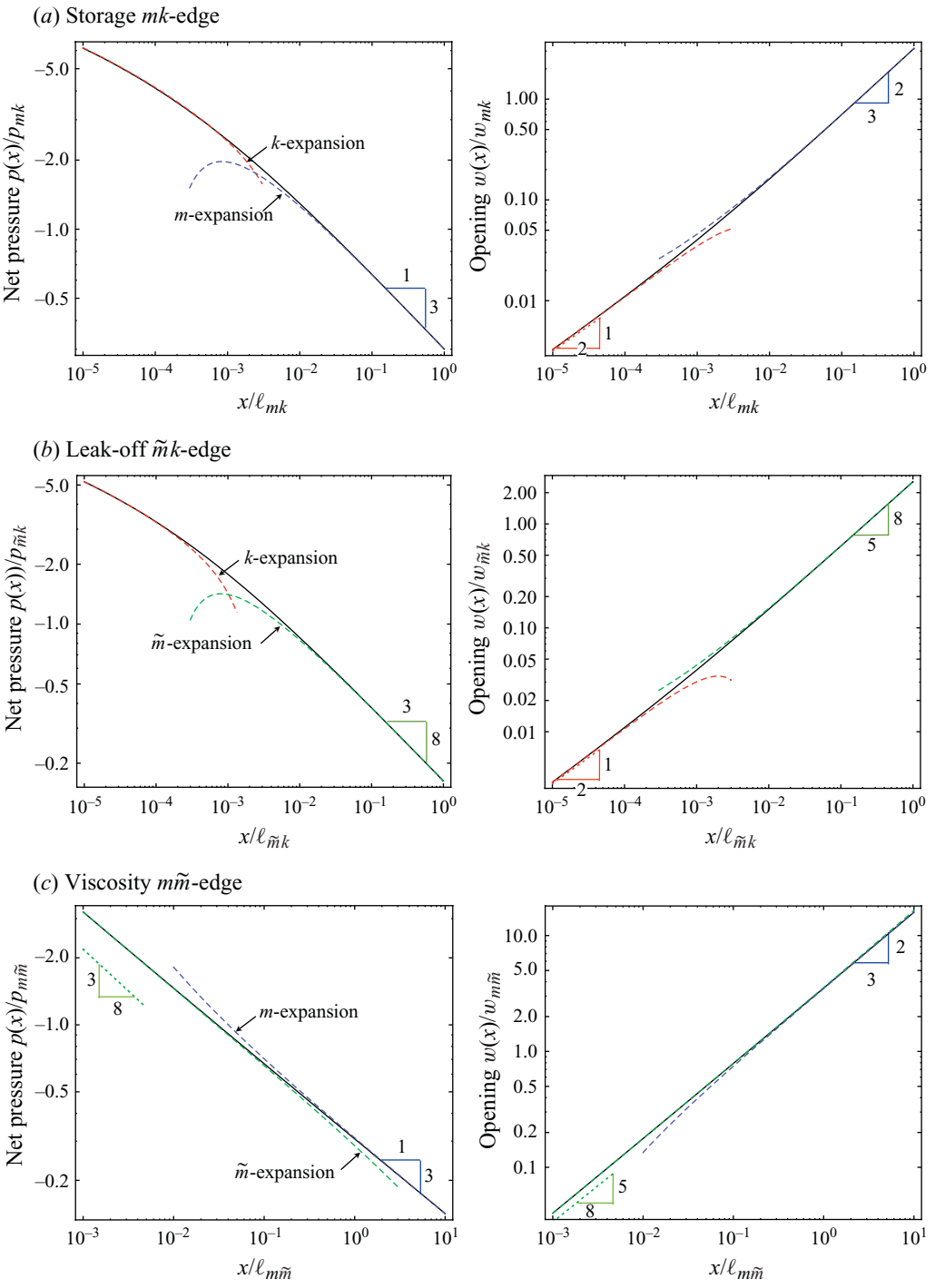


FIGURE 3. (Colour online) Net pressure and crack opening in the edge (*a*) mk, (*b*) $\tilde{m}k$ and (*c*) $m\tilde{m}$ solutions in the respective scalings. Scaling quantities are defined in table 2. Near- and far-field asymptotic expansions are shown by dashed lines.

https://doi.org/10.1017/S002211201000501X Published online by Cambridge University Press

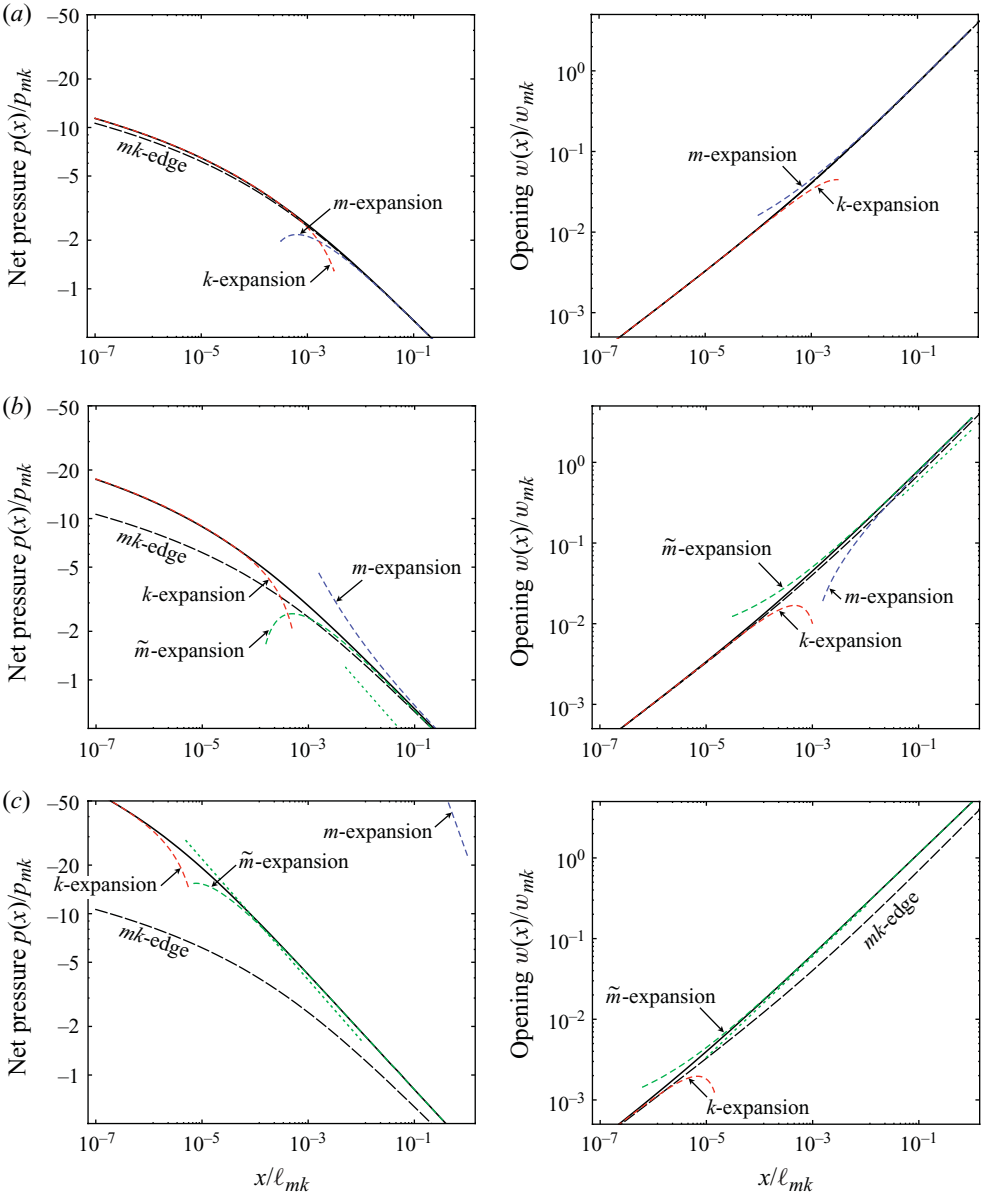


FIGURE 4. (Colour online) General solution in the mk-scaling for the net pressure (left) and crack opening (right) shows departure from the storage mk-solution with increasing number χ: (*a*) $\chi = 0.1$, (*b*) $\chi = 1$ and (*c*) $\chi = 10$. Near-, intermediate- (for $\chi \geqslant 1$) and far-field asymptotic expansions are shown by dashed lines. The intermediate $\widetilde{m}$-asymptote is shown by a dotted line in (*b*, *c*) only.

from the mk-solution remains small for $\chi = 0.1$ (figure 4*a*), but is apparent for $\chi \geqslant 1$ (figure 4*b*–*c*). Although the numerical solution for $\chi = 1$ (figure 4*b*) is far from developing the intermediate leak-off–viscosity $\widetilde{m}$-asymptote (dotted line), it is already closely approximated by the intermediate $\widetilde{m}$-expansion (which includes corrections to the $\widetilde{m}$-asymptote) for larger values of the normalized coordinate. This is a precursor to the emerging leak-off–viscosity-dominated intermediate field, which is even more

https://doi.org/10.1017/S002211201000501X Published online by Cambridge University Press

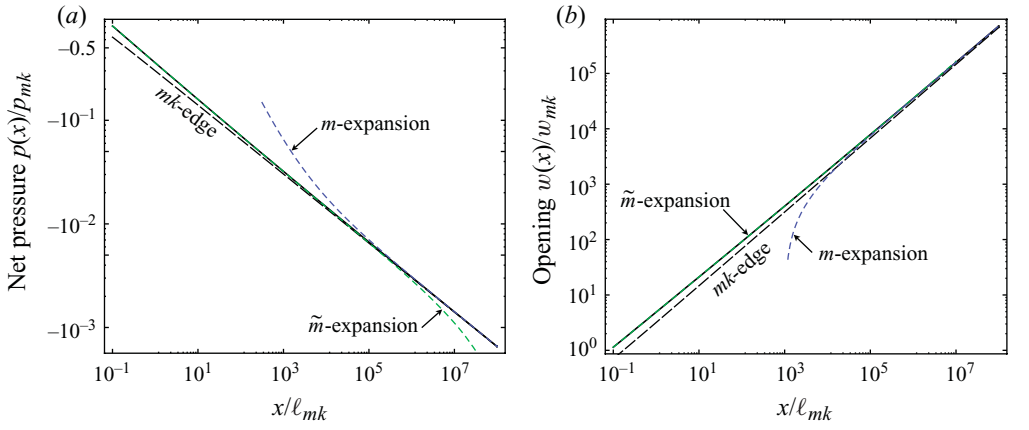


FIGURE 5. (Colour online) (*a*, *b*) Solution for $\chi = 10$ from figure 4(*c*) in the extended range of distances from the tip showing convergence towards the far-field m-expansion.

apparent for $\chi = 10$ (figure 4*c*). The increasing influence of leak-off on the solution with χ results in a widening of the transition region between the k- and m-dominated fields. This is manifested in figure 4 by a shrinking with χ of the coordinate ranges, where the solution is approximated by the k- and m-expansions. In fact, for $\chi = 10$, the far-field m-expansion is irrelevant in the coordinate range selected for figure 4(*c*). In order to trace the solution transition towards the latter, the $\chi = 10$ solution is plotted in an extended range of distances from the tip in figure 5.

Figure 6, where the net pressure and the opening are normalized with respect to the m-asymptote, presents a more detailed view of the solution for various values of χ. The emergence of the intermediate field can again be followed for successive values of $\chi \geqslant 10$, this time by contrasting the numerical solution to the $\widetilde{m}k$-edge and $m\widetilde{m}$-edge solutions shown in figure 6 (after rescaling these solutions, shown in their pertinent scalings in figure 3*b*, *c*, to the mk-scaling using (4.2)) for the three largest values of χ by medium and short dashed lines, respectively. As is evident from this comparison, the two edge solutions match over an intermediate range of distances from the tip (where both solutions possess the common $\widetilde{m}$-asymptote shown by the dotted line), when $\chi \gtrsim 100$ for the net pressure (figure 6*a*) and when $\chi \gtrsim 31$ for the opening (figure 6*b*).

The k-expansion (3.8) and m-expansion (3.10*a*, *b*), shown in figure 4 to underscore the transition of the solution between the near and far fields and its dependence on χ, rely on the numerical solution for two expansion parameters $x^o(\chi)$ and $(\beta_{-4})_k(\chi)$, respectively. These two parameters and their small and large χ asymptotics (corresponding to the edge solutions) are plotted in figure 7. Curve fitting between the limiting values given by the edge solutions, (5.1) for x^o and (5.2) with (3.12) for β_{4k}, gives simple approximations, namely $x^o(\chi) \simeq (1+\chi)^{-3}\, x^o(0) + (1+\chi^{-1})^{-4}\, x^o(\infty)$ and $(\beta_{-4})_k(\chi) \approx (1+\chi)^{-3/2}\, (\beta_{-4})_k\,(0) + \chi^{4-6h}\, (\beta_{-4})_{\widetilde{m}}\,(\infty)$ with a maximum error of 5 and 0.5 %, respectively.

5.4. *Asymptotic bounds*

In order to assess the actual extent of the various asymptotic fields, we define as an asymptotic bound the distance from the tip at which the crack opening deviates by 1 % from an asymptotic solution. Thus, $0 < x < x_0$ corresponds to the effective range

https://doi.org/10.1017/S002211201000501X Published online by Cambridge University Press

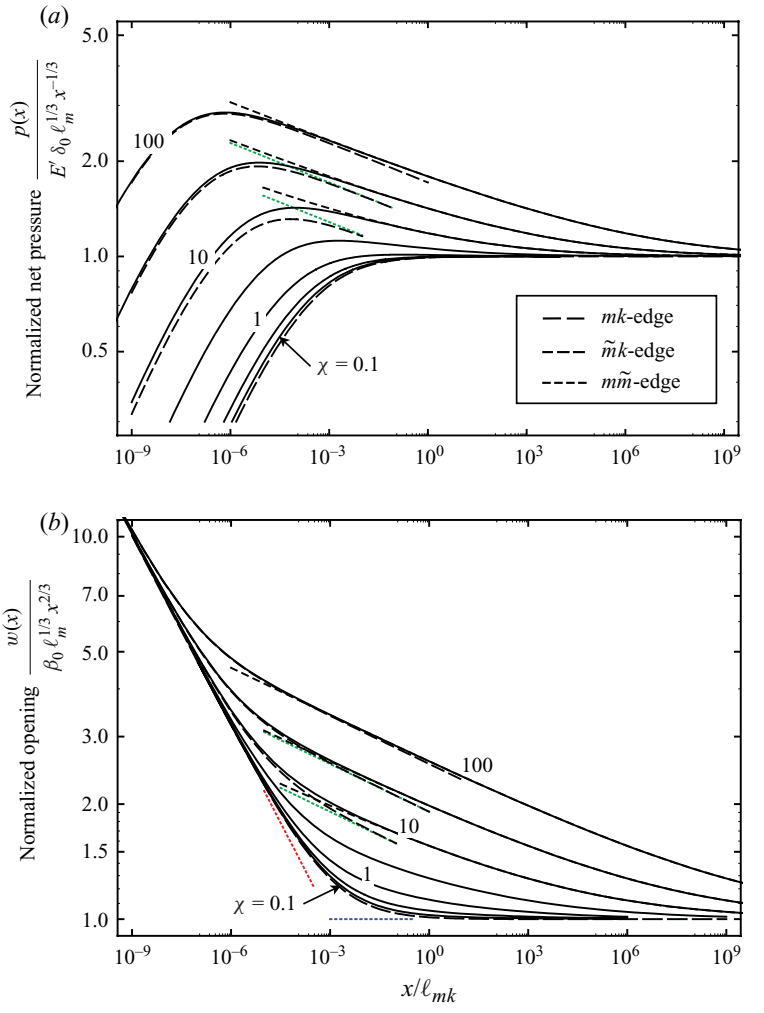


FIGURE 6. (Colour online) General solution in the mk-scaling: (a) net pressure and (b) crack opening normalized by the far-field m-asymptote for various values of number $\chi = \{0.1, 0.316, 1, 3.16, 10, 31.6, 100\}$. Dashed and dotted lines show various edge and vertex solutions, respectively.

of application of the k-asymptote, while $x > x_\infty$ is the region where the m-asymptote applies, and $\tilde{x}_\infty < x < \tilde{x}_0$ is the region (when it exists) of application of the intermediate $\widetilde{m}$-asymptote (figure 8).

The bounds of the transition interval $x \in (x_0, x_\infty)$, outside which the crack opening solution is given by the k-or m-asymptote within a 1 % accuracy,

$$4\pi \left(\frac{1}{\ell_{mk}^{1/2}} + \frac{1}{\ell_{\tilde{m}k}^{1/2}} \right) x_0^{1/2} = 1\,\%, \tag{5.4}$$

$$\frac{1}{\beta_0} \left[\sum_{j=1}^{3} \beta_{-j} \left(\frac{\ell_{m\tilde{m}}}{x_\infty} \right)^{j/6} + (\beta_{-4})_k(\chi) \left(\frac{\ell_{mk}}{x_\infty} \right)^{2/3-h} \right] = 1\,\%, \tag{5.5}$$

https://doi.org/10.1017/S0022112010000501X Published online by Cambridge University Press

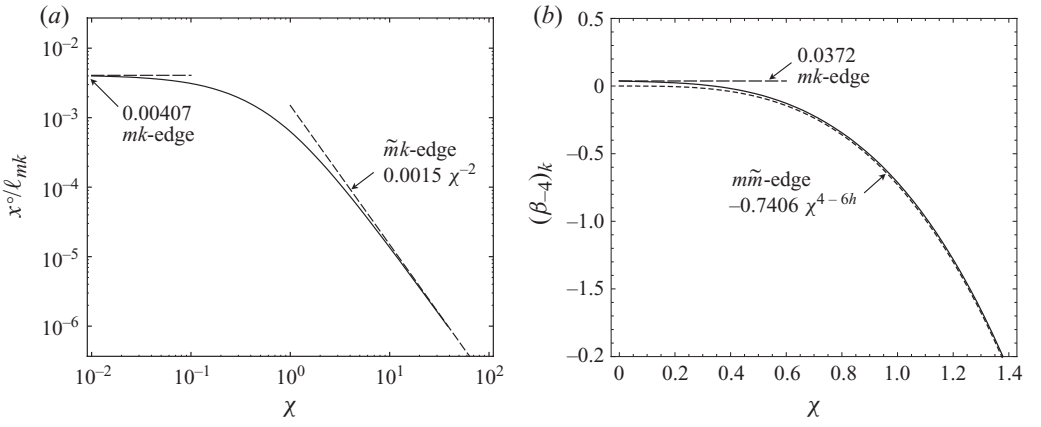


FIGURE 7. (Colour online) (*a*, *b*) Parameters x^o and $(\beta_{-4})_k$ of the near- (3.8) and far- (3.10*a*, *b*) field expansions, respectively, as a function of the dimensionless number χ.

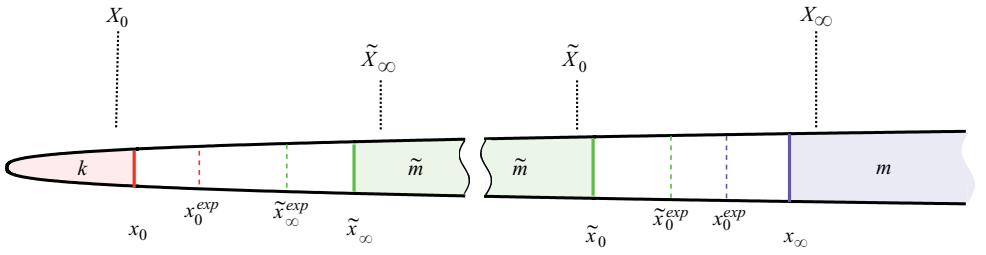


FIGURE 8. (Colour online) Sketch of a crack with bounds of the near (x_0), far (x_∞) and intermediate ($\tilde{x}_\infty$ and $\tilde{x}_0$) asymptotic fields shown. Dashed lines indicate the bounds of corresponding asymptotic expansions. Computational bounds X are rooted in their respective asymptotic fields.

are evaluated by comparing the corrective terms in expansions (3.8) and (3.10*a*, *b*) with the appropriate leading terms. In the case of the far-field bound x_∞, all four corrective terms (three leak-off terms under the sum sign and the fourth leak-off–toughness corrective term) are retained in (5.5), since the balance between the toughness term and the leak-off terms shifts from the former to the latter with increasing χ. Small χ asymptotics of (5.4) and (5.5) correspond to the near- and far-field bounds in the *mk*-edge solution, and are evaluated from the respective dominant terms, i.e. the first term in (5.4) for x_0 and the last term in (5.5) for x_∞,

$$x_0(0) = 6.3\ 10^{-7}\,\ell_{mk}, \quad x_\infty(0) \simeq 1.34\,\ell_{mk}. \tag{5.6}$$

The large χ asymptotics of (5.4) and (5.5) correspond to the near-field bound in the $\tilde{m}k$-edge solution and the far-field bound in the $m\tilde{m}$-edge solution, respectively, and are determined from the second term in (5.4) and the first term in (5.5), respectively,

$$x_0\,(\infty) = 6.3\ 10^{-7}\,\ell_{\tilde{m}k}, \quad x_\infty\,(\infty) \simeq 1.6\ 10^{7}\,\ell_{m\tilde{m}}. \tag{5.7}$$

The interval $x \in (\tilde{x}_\infty, \tilde{x}_0)$ provides a measure of the spatial extent of the intermediate $\tilde{m}$ field in the general large χ solution. The bounds $\tilde{x}_\infty$ and $\tilde{x}_0$ are computed by comparing the leading term to the next-order toughness and storage terms in the

https://doi.org/10.1017/S002211201000501X Published online by Cambridge University Press

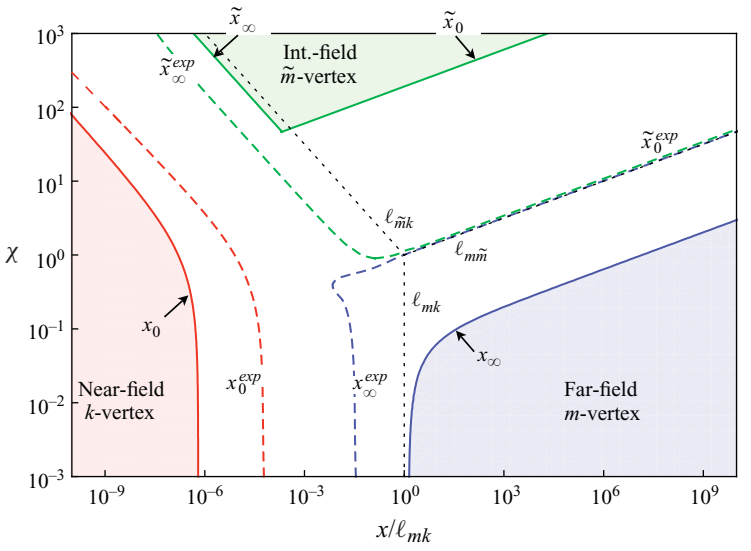


FIGURE 9. (Colour online) Dependence of the asymptotic bounds on dimensionless number χ quantifying departure of the solution from the storage mk-edge.

$\tilde{m}$-expansion (3.13a, b), respectively,

$$\frac{\tilde{\beta}_{-1}}{\tilde{\beta}_0}\left(\frac{\ell_{\tilde{m}k}}{\tilde{x}_\infty}\right)^{5/8-\tilde{h}} = 1\,\% \quad \Rightarrow \quad \tilde{x}_\infty \simeq 0.44\,\ell_{\tilde{m}k}, \tag{5.8}$$

$$\frac{\tilde{\beta}_1}{\tilde{\beta}_0}\left(\frac{x_0}{\ell_{m\tilde{m}}}\right)^{1/8} = 1\,\% \quad \Rightarrow \quad \tilde{x}_0 = 2\times 10^{-14}\,\ell_{m\tilde{m}}. \tag{5.9}$$

On the basis of these asymptotic thresholds, a map of the solution various asymptotic regions and their dependence on χ can be constructed: see figure 9. The figure also shows the interval (x_0, x_∞), as well as the intermediate-field interval $(\tilde{x}_\infty, \tilde{x}_0)$ for large χ. The length scales ℓ_{mk}, $\ell_{\tilde{m}k}$ and $\ell_{m\tilde{m}}$, which scale the asymptotic bounds for either small or large values of χ, are shown by dotted lines.

An additional set of asymptotic thresholds, x_0^{exp}, x_∞^{exp}, $\tilde{x}_\infty^{exp}$ and $\tilde{x}_0^{exp}$, is defined by requiring that the crack opening solution is given there with 1 % accuracy by the respective asymptotic expansions (rather than their leading asymptotic terms only). Naturally, the latter define reduced transition regions, such that $(x_0^{exp}, x_\infty^{exp}) \subset (x_0, x_\infty)$, $(x_0^{exp}, \tilde{x}_\infty^{exp}) \subset (x_0, \tilde{x}_\infty)$ and $(\tilde{x}_0^{exp}, x_\infty^{exp}) \subset (\tilde{x}_0, x_\infty)$. These reduced transition regions ought to be embedded into the respective computational intervals. The small χ limit

$$\chi = 0: \quad x_0^{exp}(0) \simeq 5.7\ 10^{-5}\,\ell_{mk}, \quad x_\infty^{exp}(0) \simeq 0.034\,\ell_{mk} \tag{5.10}$$

and the large χ limit

$$x_0^{exp}(\infty) \simeq 3.2\ 10^{-5}\,\ell_{\tilde{m}k}, \quad \tilde{x}_\infty^{exp} \simeq 0.024\,\ell_{\tilde{m}k}, \quad \tilde{x}_0^{exp} \simeq 0.64\,\ell_{m\tilde{m}}, \quad x_\infty^{exp}(\infty) \simeq 1.04\,\ell_{m\tilde{m}} \tag{5.11}$$

of these bounds were evaluated numerically from the respective edge solutions. Evolution of the expansion bounds with χ (between the limiting values given above) was computed from the general numerical solution and shown in figure 9 by dashed lines. It is also evident from figure 9 that the emergence of the intermediate, leak-off–viscosity-dominated field for $\chi \sim 100$ is already anticipated in the numerical solution for $\chi \gtrsim 1$, when the $\tilde{m}$-expansion provides an adequate approximation at the

https://doi.org/10.1017/S002211201000501X Published online by Cambridge University Press

intermediate distances from the tip, $\tilde{x}_\infty^{exp} < x < \tilde{x}_0^{exp}$. In addition, the $m\widetilde{m}$-edge solution, which is one of the two parts of the composite solution for large χ, is given by its two (the $\widetilde{m}$- and m-) expansions practically in the entire corresponding coordinate range, as the corresponding asymptotic thresholds $\tilde{x}_0^{exp}$ and x_∞^{exp} are very close, (5.11) and figure 9. The latter feature is also evident from the plot of corresponding net pressure and crack opening in the $m\widetilde{m}$-edge solution with the respective expansions in figure 3(*c*).

6. Dominant tip asymptotics

The steadily propagating semi-infinite hydraulic fracture solution presented in this paper defines the dominant asymptotic behaviour near the leading edge of a finite, 'parent' fracture provided that the relevant transition length scale, ℓ_{mk}, $\ell_{m\tilde{m}}$ or $\ell_{\tilde{m}k}$ (function of the tip velocity), is either much smaller or much larger than the characteristic length $\ell(t)$ that most appropriately describes the finite fracture in the neighbourhood of the tip; and that the tip velocity V does not change appreciably over crack propagation distances of the order of the transition length scale. The characteristic length $\ell(t)$ could be, for example, the local radius of curvature of the fracture edge, or the distance to the fluid source or a length characterizing the spatial variation of the solid properties or the far-field stress. For example, when both length scales associated with the transition to the storage–viscosity m-asymptote (i.e. ℓ_{mk} and $\ell_{m\tilde{m}}$) in the semi-infinite crack solution are small compared with ℓ, the effects of toughness and leak-off on the fracture scale ℓ are also small; the fracture propagation regime is then defined by the dominant m-asymptote near the leading edge.

We can identify three primary regimes of propagation in reference to the dominant tip asymptotics: (i) storage–viscosity regime ($\ell_{mk}, \ell_{m\tilde{m}} \ll \ell$), (ii) leak-off–viscosity regime ($\ell_{\tilde{m}k} \ll \ell \lesssim \ell_{m\tilde{m}}$) and (iii) toughness regime ($\min\{\ell_{mk}, \ell_{\tilde{m}k}\} \gtrsim \ell$). As the tip velocity V and/or the length scale ℓ may vary along the fracture edge, the above regimes are defined locally. A global fracture propagation regime can be defined only when the conditions for a particular local regime are met everywhere along the fracture edge. In the particular cases of a plane strain and a radial hydraulic fracture, the local and global propagation regimes are obviously identical.

The regime of fluid-driven fracture propagation evolves based on the changing nature of the dominant tip process, defined by the relation between the three transition tip length scales ℓ_{mk}, $\ell_{m\tilde{m}}$, $\ell_{\tilde{m}k}$, and the length scale ℓ of the finite crack. In the three limiting regimes introduced above, the dominant tip asymptotics (which controls the outer fracture solution on length scale ℓ) is given by the m-, $\widetilde{m}$- and k-asymptotes, respectively. Each of these three regimes of propagation and small deviations from these regimes with regard to the non-dominant processes are discussed next.

6.1. *Storage–viscosity-dominated propagation* ($\ell_{mk}, \ell_{m\tilde{m}} \ll \ell$)

The semi-infinite hydraulic fracture corresponds to a boundary layer of thickness $d \equiv \max\{\ell_{mk}, \ell_{m\tilde{m}}\}$ near the leading edge of the finite fracture, provided that $d \ll \ell$. The effects of toughness and leak-off are localized into the tip boundary layer, while the far-field asymptotics of the boundary layer, the m-solution, captures the behaviour of the outer solution near the fracture tip. These types of outer solutions have been explicitly constructed for plane strain and penny-shaped hydraulic fractures (Carbonell *et al.* 1999; Adachi & Detournay 2002; Savitski & Detournay 2002). The condition $d \ll \ell$ implies matching of the boundary-layer solution with the outer solution for the parent fracture in the range of distances from the tip, $d \ll x \ll \ell$, where both solutions possess the common m-asymptote.

https://doi.org/10.1017/S002211201000501X Published online by Cambridge University Press

The effect of the non-dominant processes (i.e. of the toughness and leak-off) onto the otherwise storage–viscosity-dominated propagation of the parent fracture stems from the next-order terms in the far-field m-expansion (3.10a, b) of the tip boundary layer. By accounting for these terms, the toughness and leak-off perturbations of the outer solution can be determined explicitly, at least for a simple fracture geometry (Garagash & Detournay 2005; Adachi & Detournay 2008).

Furthermore, the above realization that the information about the non-dominant tip processes is 'communicated' to the outer fracture solution via the next-order terms in the boundary-layer m-expansion allows us to quantify these effects onto the parent fracture in a universal manner (i.e. for any parent fracture geometry, variable *in situ* stress and properties of the solid, fluid injection conditions, etc.). Indeed, let us write the boundary-layer thickness normalized by the local parent fracture length scale ℓ as

$$\frac{d}{\ell} = \max\{\mathscr{K}_m^6, \mathscr{C}_m^6\}, \tag{6.1}$$

where

$$\mathscr{K}_m = \left(\frac{\ell_{mk}}{\ell}\right)^{1/6} = \frac{K'}{E'^{2/3}\,\mu'^{1/3}\,V^{1/3}\,\ell^{1/6}}, \qquad \mathscr{C}_m = \left(\frac{\ell_{m\tilde{m}}}{\ell}\right)^{1/6} = \frac{C'\,E'^{1/3}}{\mu'^{1/3}\,V^{5/6}\,\ell^{1/6}}, \tag{6.2a, b}$$

are the dimensionless toughness and leak-off parameters, respectively, on the scale of the parent fracture. A parameter $\mathscr{E}_m$, which quantifies the effects of the solid toughness and fluid leak-off onto the outer solution, or, in other words, the departure of the outer solution from its zero-toughness, zero-leak-off limit due to these effects, can then be defined by contrasting the next-order terms to the leading-order term in the boundary-layer far-field m-expansion (3.10a, b) at distances from the tip representative of the parent crack scale, i.e. at $x \sim \ell$,

$$\mathscr{E}_m = \beta_{-1}\,\mathscr{C}_m + \beta_{-2}\,\mathscr{C}_m^2 + \beta_{-3}\,\mathscr{C}_m^3 + (\beta_{-4})_k\,(\chi)\,\mathscr{K}_m^{4-6h}, \quad \left(4-6h \simeq 3.18, \quad \chi = \frac{\mathscr{C}_m}{\mathscr{K}_m}\right). \tag{6.3}$$

In the above, the $O(1)$ numeric coefficients β_{-j} $(j = 1, 2, 3)$ are given by (3.11), and $(\beta_{-4})(\chi)$ in figure 7(b).

6.2. *Leak-off–viscosity-dominated propagation* ($\ell_{\tilde{m}k} \ll \ell \lesssim \ell_{m\tilde{m}}$)

In this case, the fluid leak-off is dominant and thus no longer localized into the tip region of the fracture, while the effect of the solid toughness is small enough to be localized at the tip. Here the solution is again characterized by a tip boundary-layer structure, but this time of thickness $d \equiv \ell_{\tilde{m}k}$. The boundary layer corresponds to the $\tilde{m}k$-edge solution of a semi-infinite fracture. The effect of the toughness on the outer solution can thus be neglected in a first approximation; hence, the asymptotic behaviour of the outer solution near the fracture tip is given by the $\tilde{m}$-asymptote, which is prescribed there by matching with the far-field asymptotics of the boundary-layer solution.

Similar to the treatment of the storage–viscosity-dominated case, the non-dominant effect of the solid toughness and fluid storage in the crack on the otherwise leak-off–viscosity-dominated outer solution stems from the corrective terms in the $\tilde{m}$-expansion (3.13a, b) of the boundary-layer solution. A measure $\mathscr{E}_{\tilde{m}}$ of this departure is given by the ratio of the corrective terms to the leading term in (3.13a, b), evaluated at the

https://doi.org/10.1017/S0022112010000501X Published online by Cambridge University Press

parent crack scale, $x \sim \ell$,

$$\mathscr{E}_{\tilde{m}} = \tilde{\beta}_{-1}\, \mathscr{K}_{\tilde{m}}^{5-8\tilde{h}} + \tilde{\beta}_1\, \mathscr{S}_{\tilde{m}} + \tilde{\beta}_2\, \mathscr{S}_{\tilde{m}}^2 + \tilde{\beta}_3\, \mathscr{S}_{\tilde{m}}^3, \quad (5-8\tilde{h} \simeq 4.44), \tag{6.4}$$

where $\tilde{\beta}_{-1} \simeq 0.016$ (5.3), the $O(1)$ values of coefficients $\tilde{\beta}_{-j}$ $(j = 1, 2, 3)$ are given in (3.14), and the dimensionless toughness and storage parameters on the parent crack scale are defined as

$$\mathscr{K}_{\tilde{m}} = \left(\frac{\ell_{\tilde{m}k}}{\ell}\right)^{1/8} = \frac{K'}{E'^{3/4}\, \mu'^{1/4}\, C'^{1/4}\, V^{1/8}\, \ell^{1/8}}, \qquad \mathscr{S}_{\tilde{m}} = \left(\frac{\ell}{\ell_{m\tilde{m}}}\right)^{1/8} = \frac{\mu'^{1/4}\, V^{5/8}\, \ell^{1/8}}{C'^{3/4}\, E'^{1/4}}, \tag{6.5a, b}$$

respectively.

6.3. *Toughness-dominated propagation* ($\min\{\ell_{mk}, \ell_{\tilde{m}k}\} \gtrsim \ell$)

Here the solid toughness is the dominant cause of energy dissipation. In view of (6.2*a*) and (6.5*a*), the condition $\min\{\ell_{mk}, \ell_{\tilde{m}k}\} \gtrsim \ell$ simply means that the relevant dimensionless toughness parameter(s) in the outer solution, $\mathscr{K}_m$ or $\mathscr{K}_{\tilde{m}}$, is large. Under this condition, no boundary layer exists at the fracture tip, and the finite fracture solution is simply characterized by the dominant k-asymptote at the tip.

A measure $\mathscr{E}_k$ of the departure of the parent fracture solution from the zero-viscosity limit with increasing fluid viscosity can be assessed by evaluating the ratio of the viscosity correction terms to the leading term in the k-expansion for the crack opening (3.8) at the parent crack scale $x \sim \ell$, in the following two equivalent forms:

$$\mathscr{E}_k = 4\pi\, \mathscr{M}_k\, (1 + \mathscr{C}_k) = 4\pi\, \mathscr{M}_{\tilde{k}}\, (\mathscr{S}_{\tilde{k}} + 1). \tag{6.6}$$

Here $\mathscr{M}_k$ and $\mathscr{C}_k$ are the dimensionless viscosity and leak-off parameters on the parent crack scale, respectively,

$$\mathscr{M}_k = \left(\frac{\ell}{\ell_{mk}}\right)^{1/2} = \frac{\mu'\, E'^2 V\, \ell^{1/2}}{K'^3}, \qquad \mathscr{C}_k = \chi, \tag{6.7}$$

while $\mathscr{M}_{\tilde{k}}$ and $\mathscr{S}_{\tilde{k}}$ are alternative parameters, corresponding to the dimensionless viscosity and storage, respectively, on the parent crack scale,

$$\mathscr{M}_{\tilde{k}} = \left(\frac{\ell}{\ell_{\tilde{m}k}}\right)^{1/2} = \frac{\mu'\, C'\, E'^3 V^{1/2}\, \ell^{1/2}}{K'^4}, \quad \mathscr{S}_{\tilde{k}} = \frac{1}{\chi}. \tag{6.8}$$

The measure $\mathscr{E}_k$ reduces to either $\mathscr{M}_k$ or $\mathscr{M}_{\tilde{k}}$ (multiplied by 4π) in the limit when the fluid leak-off ($\mathscr{C}_k$) or fluid storage ($\mathscr{S}_{\tilde{k}}$) in the crack is negligible, respectively.

6.4. *Estimates of the transition length scales*

Following the above discussion, the magnitude of the transition length scales and their relation to the finite fracture length define the dominant tip asymptotics and the corresponding propagation regime. In order to illustrate the range of variation and the relative magnitudes of these length scales, we consider as a departure point values of material parameters that are characteristic of petroleum field applications; namely, rock toughness $K_{Ic} = 1$ MPa m$^{1/2}$, modulus $E' = 30$ GPa, fracturing fluid viscosity $\mu = 100$ cP, and leak-off coefficient C_L in the range between 10^{-5} and 10^{-4} m s$^{-1/2}$. To estimate the fracture propagation velocity, we consider the solution for the radius of a penny-shaped, fluid-driven fracture under conditions of zero toughness, leak-off and lag (Savitsky & Detournay 2002), $\ell(t) \simeq 0.698(E' Q_o^3/\mu')^{1/9} t^{4/9}$. Assuming a value of the constant rate of fluid injection at the crack centre, $Q_o = 0.03$ m^3 s^{-1}, we observe

https://doi.org/10.1017/S002211201000501X Published online by Cambridge University Press

that the tip velocity $V \approx 6$, 0.3 and 0.02 m s^{-1} when $\ell = 1$, 10 and 100 m, respectively. (Typical final fracture size in petroleum reservoir applications tends to be in the higher end of this range.) Using an average value $V \approx 0.1$ m s^{-1}, the low-end value of the leak-off coefficient and values of other parameters as defined, we can express the transition length scales as

$$\left.\begin{aligned} \ell_{mk} &\simeq \left(\frac{K_{Ic}}{1\ \text{MPa m}^{1/2}}\right)^6 \left(\frac{0.1\ \text{m s}^{-1}}{V}\frac{100\ \text{cP}}{\mu}\right)^2 \left(\frac{30\ \text{GPa}}{E'}\right)^4 0.09\ \text{m}, \\ \ell_{m\tilde{m}} &\simeq \left(\frac{C_L}{10^{-5}\ \text{m s}^{-1/2}}\right)^6 \left(\frac{0.1\ \text{m s}^{-1}}{V}\right)^5 \left(\frac{100\ \text{cP}}{\mu}\right)^2 \left(\frac{E'}{30\ \text{GPa}}\right)^2 0.004\ \text{m}. \end{aligned}\right\} \tag{6.9}$$

Therefore, for the chosen values of the parameters, $\ell_{mk} \simeq 9$ cm is much larger than $\ell_{m\tilde{m}}$, implying the storage–viscosity regime of the fracture propagation as long as the fracture extent $\ell \gg 9$ cm. Estimate of the maximum fluid lag under zero-leak-off conditions (Garagash & Detournay 2000), expressed in terms similar to (6.9),

$$\ell_{lag} \simeq \left(\frac{30\ \text{MPa}}{\sigma_o}\right)^3 \left(\frac{E'}{30\ \text{GPa}}\right)^2 \left(\frac{V}{0.1\ \text{m s}^{-1}}\frac{\mu}{100\ \text{cP}}\right) 0.0014\ \text{m}, \tag{6.10}$$

where 30 MPa is used as a characteristic value for the confining stress σ_o, validates the assumption of the negligible fluid lag for this case, i.e. $\ell_{lag} \ll \ell_{mk}$.

Variation in some of the parameters (e.g. C_L and V) within a plausible range may completely alter the propagation regime. For example, $\ell_{m\tilde{m}}$ increases by six orders of magnitude with increase of C_L by one order to the high-end value 10^{-4} m s$^{-1/2}$, while values of $\ell_{m\tilde{m}}$ and ℓ_{lag} are not affected by this change (6.9), resulting in the leak-off–viscosity-dominated propagation regime. Similarly, an increase in the value of the tip velocity by one order of magnitude to 1 m s^{-1}, which is representative of earlier propagation stages (shorter fracture), results in decrease of ℓ_{mk} and $\ell_{m\tilde{m}}$ by two and five orders of magnitude, respectively (6.9), and an increase of ℓ_{lag} by one order of magnitude (6.10), which suggests that fluid lag would be the dominant process in this case (e.g. Garagash 2006*b*, 2009).

7. Regimes of propagation of particular finite fractures

We apply the above considerations on the dominant tip asymptotes to establish the link between the tip asymptotics and the global regimes of propagation for plane strain and radial fractures. We also briefly discuss the construction of numerical algorithms that can automatically account for the dominant tip process.

7.1. *Plane-strain hydraulic fracture*

A plane-strain fracture normally develops as a result of fluid injection from a line source in an unbounded solid medium under a homogeneous state of stress. Here $\ell(t)$ is the fracture half-length. The $O(1)$ outer solutions in the four limiting propagation regimes that are dominated by one of the two fluid balance processes and one of the two dissipative processes are known when the fluid injection rate is a constant, Q_o; see table 4 for a list of the corresponding expressions for $\ell(t)$. Using these expressions for ℓ and the resulting tip propagation velocity, $V = \mathrm{d}\ell/\mathrm{d}t$, the pairs of dimensionless parameters quantifying the non-dominant processes for a given limiting propagation regime can be identified by evaluating the universal expressions (6.2*a*, *b*), (6.5*a*, *b*), (6.7) and (6.8). (For example, the expression for $\ell(t)$ in the storage–viscosity-dominated

https://doi.org/10.1017/S002211201000501X Published online by Cambridge University Press

Limiting regime	$O(1)$ solution for the Griffith half-length ℓ	Parameters of the non-dominant processes ($O(1)$ numerical coefficients are omitted)
Storage–viscosity	$0.615\left(\dfrac{E'\,Q_o^3}{\mu'}\right)^{1/6} t^{2/3}$ (Carbonell *et al.* 1999)	(6.2*a*, *b*): $\mathscr{K}_m = \dfrac{K'}{E'}\left(\dfrac{E'}{\mu' Q_o}\right)^{1/4}$ $\mathscr{C}_m = C'\left(\dfrac{E' t}{\mu' Q_o^3}\right)^{1/6}$
Leak-off–viscosity	$\dfrac{1}{\pi}\dfrac{Q_o}{C'} t^{1/2}$ (Adachi & Detournay 2008)	(6.5*a*, *b*): $\mathscr{K}_{\tilde{m}} = \dfrac{K'}{E'}\left(\dfrac{E'}{\mu' Q_o}\right)^{1/4}$ $\mathscr{S}_{\tilde{m}} = \dfrac{1}{C'^{3/2}}\left(\dfrac{\mu' Q_o^3}{E' t}\right)^{1/4}$
Storage–toughness	$\dfrac{2}{\pi^{2/3}}\left(\dfrac{E'\,Q_o}{K'}\right)^{2/3} t^{2/3}$ (Garagash 2006*a*)	(6.7): $\mathscr{M}_k = \dfrac{\mu'\,E'^3 Q_o}{K'^4}$ $\mathscr{C}_k = C'\left(\dfrac{E'^4 t}{K'^4 Q_o^2}\right)^{1/6}$
Leak-off–toughness	$\dfrac{1}{\pi}\dfrac{Q_o}{C'} t^{1/2}$ (Bunger *et al.* 2005)	(6.8): $\mathscr{M}_{\tilde{k}} = \dfrac{\mu'\,E'^3 Q_o}{K'^4}$ $\mathscr{S}_{\tilde{k}} = \dfrac{1}{C'^{3/2}}\left(\dfrac{K'^4 Q_o^2}{E'^4 t}\right)^{1/4}$

TABLE 4. Four limiting propagation regimes of a Griffith fluid-driven fracture and corresponding dimensionless parameters quantifying the effects of the non-dominant tip processes for each regime.

propagation regime, Carbonell *et al.* 1999, is used in (6.2*a*, *b*) to evaluate the toughness $\mathscr{K}_m$ and leak-off $\mathscr{C}_m$ dimensionless parameters on the Griffith crack scale.)

We can confirm that the parameters in table 4 are identical to those obtained from independent scaling considerations (references cited in this paragraph). The available outer solutions for various perturbations of the limiting propagation regimes also confirm that $\mathscr{E}_m$, $\mathscr{E}_{\tilde{m}}$ and $\mathscr{E}_k$ are the relevant measures of the respective perturbations. Indeed, explicit outer solutions for the independent toughness (Garagash & Detournay 2005) and leak-off (Adachi & Detournay 2008) perturbations of the storage–viscosity-dominated regime show that the reduced expressions for $\mathscr{E}_m$ given by (6.3), i.e. $0.037\,\mathscr{K}_m^{3.18}$ (when $\mathscr{C}_m = 0$) and $0.5\,\mathscr{C}_m$ (when $\mathscr{K}_m = 0$), provide the exact dependence of these perturbed solutions on the toughness and leak-off, respectively. Similar observations can be made for (i) the reduced expressions for $\mathscr{E}_{\tilde{m}}$ given by (6.4), i.e. $0.016\,\mathscr{K}_{\tilde{m}}^{4.44}$ (when $\mathscr{S}_{\tilde{m}} = 0$) and $1.302\,\mathscr{S}_{\tilde{m}}$ (when $\mathscr{K}_{\tilde{m}} = 0$) based on the explicit solutions for the toughness (Garagash 2010) and storage (Adachi & Detournay 2008) perturbations of the leak-off–viscosity-dominated regime, respectively; and (ii) the reduced expression for $\mathscr{E}_k$, (6.6), $4\pi\,\mathscr{M}_k$ (when $\mathscr{C}_k = 0$) and $4\pi\,\mathscr{M}_{\tilde{k}}$ (when $\mathscr{S}_{\tilde{k}} = 0$) for the viscosity perturbations of the respective toughness-dominated regimes (Garagash 2006*b*, 2010). All of the above perturbation solutions consider a perturbation from a vertex solution in only one parameter. If the corresponding perturbation measures $\mathscr{E}$ are to be evaluated in the general case when both relevant non-dominant processes have to be accounted for, then the $O(1)$ numerical prefactors, omitted in the expressions for the dimensionless parameters in table 4, have to be retained.

https://doi.org/10.1017/S002211201000501X Published online by Cambridge University Press

Limiting regime	$O(1)$ solution for radius ℓ of the penny-shaped fracture	Parameters of the non-dominant processes ($O(1)$ numerical coefficients are omitted)
Storage–viscosity	$0.698\left(\dfrac{E'Q_o^3}{\mu'}\right)^{1/9}t^{4/9}$ (Savitski & Detournay 2002)	(6.2a, b): $\mathscr{K}_m = K'\left(\dfrac{t^2}{\mu'^5 Q_o^3 E'^{13}}\right)^{1/18}$
		$\mathscr{C}_m = C'\left(\dfrac{E'^4 t^7}{\mu'^4 Q_o^6}\right)^{1/18}$
Leak-off–viscosity	$\dfrac{2^{1/2}}{\pi}\left(\dfrac{Q_o}{C'}\right)^{1/2}t^{1/4}$ (Madyarova & Detournay 2010)	(6.5a, b): $\mathscr{K}_{\tilde{m}} = K'\left(\dfrac{t}{E'^{12}\mu'^4 C'^2 Q_o^2}\right)^{1/16}$
		$\mathscr{S}_{\tilde{m}} = \dfrac{1}{C'^{9/8}}\left(\dfrac{\mu'^4 Q_o^6}{E'^4 t^7}\right)^{1/16}$
Storage–toughness	$\left(\dfrac{9}{2\pi^2}\right)^{1/5}\left(\dfrac{E'Q_o}{K'}\right)^{2/5}t^{2/5}$ (Savitski & Detournay 2002)	(6.7): $\mathscr{M}_k = \mu'\left(\dfrac{Q_o^3 E'^{13}}{K'^{18}t^2}\right)^{1/5}$
		$\mathscr{C}_k = C'\left(\dfrac{E'^8 t^3}{K'^8 Q_o^2}\right)^{1/10}$
Leak-off–toughness	$\dfrac{2^{1/2}}{\pi}\left(\dfrac{Q_o}{C'}\right)^{1/2}t^{1/4}$ (Bunger *et al.* 2005)	(6.8): $\mathscr{M}_{\tilde{k}} = \mu'\left(\dfrac{E'^{12}C'^2Q_o^2}{K'^{16}t}\right)^{1/4}$
		$\mathscr{S}_{\tilde{k}} = \dfrac{1}{C'^{5/4}}\left(\dfrac{K'^8 Q_o^2}{E'^8 t^3}\right)^{1/8}$

TABLE 5. Four limiting propagation regimes of a penny-shaped fluid-driven fracture and corresponding dimensionless parameters quantifying the effects of the non-dominant tip processes for each regime.

7.2. *Penny-shaped hydraulic fracture*

If the fracturing fluid is injected in an infinite medium under a homogeneous state of stress, from a point source rather than from a line source, the resulting fracture will be penny-shaped, with $\ell(t)$ now denoting the fracture radius. For a constant injection rate, there exist again four primary asymptotic regimes, which correspond to similarity solutions of the system of equations governing the fracture propagation; see table 5 for a list of the similarity solutions for $\ell(t)$.

These expressions for $\ell(t)$, in conjunction with the universal expressions (6.2a, b), (6.5a, b), (6.7) and (6.8), again yield the pairs of dimensionless parameters quantifying the non-dominant processes for each primary propagation regime. These parameters, which are listed in table 5, are identical to those obtained from independent scaling considerations (Detournay & Garagash 2010). In contrast to the plane-strain case, however, all the parameters are now dependent on time, a reflection of the existence of two independent time scales instead of one in the previous case. As a result, the dominant regime of propagation of a radial fracture is viscosity–storage at time small relative to these two time scales, but leak-off–toughness at time large compared to both scales. The appearance of the two other regimes, as intermediate time asymptotics, hinges on the separation of the two time scales, with their ordering deciding whether the viscosity–leak-off or the toughness–storage becomes visible at times intermediate between the two scales.

https://doi.org/10.1017/S002211201000501X Published online by Cambridge University Press

7.3. *Tip region in the numerical solutions of hydraulic fractures*

The significance of the tip region to the overall fracture solution raises the important issue of how to resolve numerically the solution in the vicinity of the fracture front. A further challenge in answering this question is the changing nature of the dominant tip process, which causes the fracture to evolve through a sequence of limiting regimes. Two different approaches can be suggested: (i) use of the single, toughness-dominated tip asymptote in the numerical solution (Spence & Sharp 1985; Hu & Garagash 2010); (ii) use of the mapping of the complete semi-infinite fluid-driven fracture solution onto the tip region of the finite parent fracture to provide for continuous change of the dominant tip asymptote (Adachi & Detournay 2008; Peirce & Detournay 2008). The first method requires the use of numerical discretization interval $\Delta\ell$ in the parent fracture, which would allow us to resolve the toughness-dominated near-tip region, i.e. $\Delta\ell \ll \min\{\ell_{mk}, \ell_{\tilde{m}k}\}$. The latter can easily prove to be exceedingly small and computationally inefficient when the fracture is, say, in the viscosity-dominated regime. (For numerical methods based on the solution series expansion over a class of functions with the given tip behaviour, the first method requires the use of an exceedingly large number of terms in the series to resolve the toughness asymptote on a vanishingly small tip length scale during the viscosity-dominated propagation (Spence & Sharp 1985), which also leads to a poor series convergence.) The second approach allows for a larger discretization length, and thus yields more efficient numerical methods. It has been successfully implemented to solve numerically for the evolution of Griffith's hydraulic fracture from the storage to the leak-off-dominated regimes under conditions of zero rock toughness (Adachi & Detournay 2008), and for the evolution of a penny-shaped hydraulic fracture from the storage–viscosity to the leak-off–toughness-dominated regimes (Madyarova & Detournay 2010).

8. Conclusions

The near-tip region of a hydraulic fracture propagating in a permeable elastic solid has been analysed by considering the related problem of a semi-infinite steadily moving crack. The analysis builds on previous solutions of this problem, which are shown to be particular cases of the general solution derived here. In fact, an important result of this paper is a demonstration of the existence of two independent length scales (e.g. ℓ_{mk} and $\ell_{\tilde{m}k}$), which both depend on the tip velocity, to characterize the near-tip processes. This multiscale nature of the tip asymptotics is encapsulated in a conceptual representation of the solution in the parametric $m\tilde{m}k$-space. In this representation, the k-vertex embodies the classical LEFM asymptote, which describes the near-field solution ($x/\ell_{mk} \ll 1$), while the m-vertex represents the viscosity asymptote, which applies in the far-field ($x/\ell_{mk} \gg 1$). The spatial variation of the solution between these two asymptotes depends on the ratio of two length scales $\chi^2 = \ell_{mk}/\ell_{\tilde{m}k}$. If this ratio is large enough, there is a separation of the two length scales ℓ_{mk} and $\ell_{\tilde{m}k}$ and the solution is further characterized by the intermediate leak-off asymptote (corresponding to the $\tilde{m}$-vertex); in that case, there are three regions (near-, intermediate- and far-field) where the aperture has a power-law dependence on the distance from the tip x. Previously published solutions, besides the classical LEFM asymptote (k-vertex), correspond to the m-vertex (Desroches *et al.* 1994), the $\tilde{m}$-vertex (Lenoach 1995), the mk-edge (Garagash & Detournay 2000, 2005) that is applicable to the particular case of an impermeable medium ($\chi = 0$), and the $m\tilde{m}$-edge (Adachi & Detournay 2008). Interestingly, the theoretical mk-edge solution has recently been confirmed experimentally in laboratory experiments involving the propagation of hydraulic cracks in polymethyl methacrylate and glass specimens (Bunger & Detournay 2008).

https://doi.org/10.1017/S002211201000501X Published online by Cambridge University Press

This solution provides a framework to understand the interaction of representative physical processes near the fracture tip and to track the changing nature of the dominant tip process(es) with the tip velocity. Furthermore, it gives a universal scaling of the near-tip processes on the scale of the entire fracture and sets the foundation for developing efficient numerical algorithms relying on accurate modelling of the tip region.

We acknowledge partial support from the National Science and Engineering Research Council of Canada to D.G. under Discovery grant no. 371606 and from the National Science Foundation to E.D. under grant no. 0600058. Any opinions, findings and conclusions or recommendations expressed in this material are those of the authors and do not necessarily reflect the views of the National Science Foundation. The authors also acknowledge the contribution of Olga Kresse to the development of the numerical solution.

Appendix A. Monomial form (3.1) as near- or far-field asymptote of (2.3)

A.1. *Far field*

Let us assume that the crack opening possesses a monomial far-field asymptote $w = B\,x^{\lambda}$ $(0<\lambda<1)$, $x\to\infty$, in the sense that

$$\forall\,\varepsilon>0 \quad \exists\, X_\infty(\varepsilon)\in(0,\infty):\quad |1-w(x)/(B\,x^{\lambda})|<\varepsilon \quad \text{for} \quad \forall\, x>X_\infty. \tag{A 1}$$

The elasticity integral can then be decomposed as

$$\mathscr{L}[w](x) = I_\lambda(x) + \Delta I(x, X_\infty(\varepsilon)), \tag{A 2}$$

where

$$\left.\begin{aligned} I_\lambda(x) &= \frac{1}{4\pi}\int_0^\infty \frac{\mathrm{d}(B\,s^{\lambda})}{\mathrm{d}s}\frac{\mathrm{d}s}{x-s} = B\frac{\lambda\cot\pi\lambda}{4}\,x^{\lambda-1},\\ \Delta I(x,X) &= \frac{1}{4\pi}\left(\int_0^X + \int_X^\infty\right)\frac{\mathrm{d}(w(s)-B\,s^{\lambda})}{\mathrm{d}s}\frac{\mathrm{d}s}{x-s}. \end{aligned}\right\} \tag{A 3}$$

Let us estimate $\Delta I(x, X_\infty(\varepsilon))$ for $x\gg X_\infty$. Expanding $(x-s)^{-1}$ in series for $x\gg X_\infty>s$, the first integral in the expression for $\Delta I(x, X_\infty(\varepsilon))$ can be estimated as $O\,(f(\varepsilon)/x)$, where $f(\varepsilon)$ is bounded for all $\varepsilon>0$. In view of (A 1), the second integral in $\Delta I(x, X_\infty(\varepsilon))$ can be estimated as follows:

$$\frac{1}{4\pi}\int_{X_\infty}^\infty \frac{\mathrm{d}(w(s)-B\,s^{\lambda})}{\mathrm{d}s}\frac{\mathrm{d}s}{x-s} \sim \frac{1}{4\pi}\int_{X_\infty}^\infty \frac{\mathrm{d}(\varepsilon\,B\,s^{\lambda})}{\mathrm{d}s}\frac{\mathrm{d}s}{x-s} = \varepsilon I_\lambda(x) - \frac{1}{4\pi}\int_0^{X_\infty}\frac{\mathrm{d}(\varepsilon\,B\,s^{\lambda})}{\mathrm{d}s}\frac{\mathrm{d}s}{x-s}. \tag{A 4}$$

Since $s<X_\infty\ll x$ in the remaining integral, the latter is $O\,(g(\varepsilon)/x)$, where $g(\varepsilon)$ is bounded for all $\varepsilon>0$. We therefore observe that $I_\lambda(x)$ is the dominant far-field asymptotic term in (A 2), and that monomial solution (3.1) is a valid far-field asymptote of otherwise different solution(s) of the elasticity equation (2.3).

A.2. *Near field*

Let us now assume that the crack opening possesses a monomial near-field asymptote $w = B\,x^{\lambda}$ $(0<\lambda<1)$, $x\to 0$, in the sense that

$$\forall\,\varepsilon>0 \quad \exists\, X_0(\varepsilon)>0:\quad |1-w(x)/(B\,x^{\lambda})|<\varepsilon \quad \text{for } \forall\, x\in(0,X_0). \tag{A 5}$$

https://doi.org/10.1017/S0022112010005001X Published online by Cambridge University Press

An appropriate decomposition of the elasticity integral is

$$\mathscr{L}[w](x) = I_\lambda(x) + \Delta I(x, X_0(\varepsilon)), \tag{A 6}$$

where I_λ and $\Delta I(x, X)$ are defined in (A 3). Consider estimating $\Delta I(x, X_0(\varepsilon))$ for $x \ll X_0$. In view of (A 5), the first integral in $\Delta I(x, X_0(\varepsilon))$ can be estimated as follows:

$$\begin{aligned}\frac{1}{4\pi}\int_0^{X_0} \frac{\mathrm{d}(w(s) - B\,s^\lambda)}{\mathrm{d}s}\frac{\mathrm{d}s}{x-s} &\sim \frac{1}{4\pi}\int_0^{X_0} \frac{\mathrm{d}(\varepsilon\,B\,s^\lambda)}{\mathrm{d}s}\frac{\mathrm{d}s}{x-s}\\ &= \varepsilon I_\lambda(x) - \frac{1}{4\pi}\int_{X_0}^{\infty} \frac{\mathrm{d}(\varepsilon\,B\,s^\lambda)}{\mathrm{d}s}\frac{\mathrm{d}s}{x-s} \simeq \varepsilon I_\lambda(x) + \frac{1}{4\pi}\int_{X_0}^{\infty} \frac{\mathrm{d}(\varepsilon\,B\,s^\lambda)}{\mathrm{d}s}\frac{\mathrm{d}s}{s},\end{aligned} \tag{A 7}$$

where the remaining integral simplification is warranted by $x \ll X_0 < s$. The latter integral can be evaluated explicitly and is a constant $h(\varepsilon)$, where $h(\varepsilon)$ is bounded for all $\varepsilon > 0$. Since $x \ll X_0 < s$, the second integral in $\Delta I(x, X_0(\varepsilon))$ can be approximated by a constant

$$-\frac{1}{4\pi}\int_{X_0}^{\infty} \frac{\mathrm{d}(w(s) - B\,s^\lambda)}{\mathrm{d}s}\frac{\mathrm{d}s}{s} = c(\varepsilon) \tag{A 8}$$

bounded for all $\varepsilon > 0$. We therefore observe that $I_\lambda(x)$ is the dominant near-field asymptotic term in (A 6) and that the monomial solution (3.1) is a valid near-field asymptote of otherwise different solution(s) of the elasticity equation (2.3).

Appendix B. Near-field k-expansion (3.8)

The leading term in the opening expansion for $x \to 0$ is given by the propagation condition (2.2) expressed in terms of the toughness length scale ℓ_k, $w = \ell_k^{1/2} x^{1/2}$. Use of the elasticity equation (2.3) confirms that the corresponding 'leading' term in the net pressure expansion is zero, $p/E' = \ell_k^{1/2}\mathscr{L}[s^{1/2}][x] = 0$ (see also the class of monomial elastic solutions (3.1) with $\lambda = 1/2$). Thus, the first non-zero term in the pressure expansion has to follow from the lubrication flow equations (2.7) and (2.9), combined to yield an expression for the pressure gradient written in terms of the viscosity and leak-off length scales

$$\frac{1}{E'}\frac{\mathrm{d}p}{\mathrm{d}x} = \frac{1}{w^2}\left(\ell_m + \ell_{\tilde{m}}^{3/2}\frac{x^{1/2}}{w}\right). \tag{B 1}$$

Substitution of the leading opening term into (B 1) and integration lead to

$$\frac{p}{E'} = \frac{\ell_k^{1/2}}{\ell_1^{1/2}}(\ln x - \ln x^o), \tag{B 2}$$

where $\ln x^o$ is an integration constant and the length scale ℓ_1 is given by (3.9) in terms of the transitional length scales $\ell_{mk} = \ell_k^3/\ell_m^2$ and $\ell_{\tilde{m}k} = \ell_k^4/\ell_{\tilde{m}}^3$ introduced earlier.

Let us introduce a generalized elasticity operator

$$\mathscr{F}\,[p]\,(x, X) = \frac{4}{\pi}\int_0^X K(x, s)\,p(s)\,\mathrm{d}s, \tag{B 3}$$

which reduces to $\mathscr{L}^{-1}[p](x)$ when $X \to \infty$. As long as the sought terms in the near-field expansions are local (i.e. independent of the solution details away from the tip), the $\mathscr{L}^{-1}[p](x)$ has to be asymptotically equivalent to $\mathscr{F}[p](x, X)$ as $x \to 0$ for any finite $X \gg x$. Furthermore, if X is sufficiently small, the net pressure p under the operator $\mathscr{F}$ defined above can be replaced by its near-field local expansion.

https://doi.org/10.1017/S002211201000501X Published online by Cambridge University Press

The next-order term in the opening expansion is then sought by applying the operator $\mathscr{F}$ (B 3) to the pressure expansion (B 2). Explicit expressions for $\mathscr{F}[\ln s](x, X)$ and $\mathscr{F}[1](x, X)$ are given by functions $(4/\pi)F_{\ln}(x, X)$ and $(4/\pi)F_1(x, X)$ of Garagash & Detournay (2005), respectively (see their (C 17) and (C 18)), whose $x \to 0$ asymptotic forms are $4\pi x$ and $O(x^{3/2})$, respectively. The resulting expansion for the opening reads

$$w = \ell_k^{1/2} x^{1/2} + 4\pi \frac{\ell_k^{1/2}}{\ell_1^{1/2}} x. \tag{B 4}$$

The above two steps, i.e. the use of lubrication equation asymptotics with the current form of the opening expansion to find the next-order term in the pressure expansion, followed by the use of generalized elasticity operator to find the corresponding next-order term in the opening expansion, are repeated as follows.

Substitution of (B 4) into (B 1), expansion of the result in $x \to 0$ and integration lead to the updated pressure expansion

$$\frac{p}{E'} = \frac{\ell_k^{1/2}}{\ell_1^{1/2}} \left(\ln\left(\frac{x}{x^o}\right) - 24\pi \frac{x^{1/2}}{\ell_2^{1/2}} \right), \tag{B 5}$$

where the integration constant has been absorbed in x^o and the length scale ℓ_1 is defined in (3.9). Evaluation of the next-order opening term corresponding to the last term in the pressure expansion (B 5) relies on the explicit expression for $\mathscr{F}[s^{1/2}](x, X)$ given by the function $(4/\pi)F_{3/2}(x, X)$ of Garagash & Detournay (2005, see their (C19)), whose $x \to 0$ asymptote is $-(8/3\pi)x^{3/2} \ln x + O(x^{3/2})$. Consequently, the updated opening expansion becomes

$$w = \ell_k^{1/2} x^{1/2} + 4\pi \frac{\ell_k^{1/2}}{\ell_1^{1/2}} x + 64 \frac{\ell_k^{1/2}}{\ell_1^{1/2} \ell_2^{1/2}} x^{3/2} \ln x + O(x^{3/2}). \tag{B 6}$$

Repeating the steps again, we get from the opening expansion (B 6) and lubrication (B 1) the updated pressure expansion in the form

$$\frac{p}{E'} = \frac{\ell_k^{1/2}}{\ell_1^{1/2}} \left(\ln\left(\frac{x}{x^o}\right) - 24\pi \frac{x^{1/2}}{\ell_2^{1/2}} - 192 \frac{x \ln x}{\ell_2} + O(x) \right), \tag{B 7}$$

while the corresponding term in the opening expansion relies on evaluating $\mathscr{F}[s \ln s](x, X)$ given by the function $(4/\pi)F_{2\ln}(x, X)$ of Garagash & Detournay (2005), whose $x \to 0$ asymptote is $O(x^{3/2})$ and, more importantly, is dependent on the integration limit X. This is an indication that further higher-order terms in the opening expansion are non-local (i.e. depend on the solution away from the crack tip) and therefore cannot be obtained from asymptotic considerations alone.

Appendix C. Far-field m-expansion (3.10a, b)

As discussed in § 3.4, the leading term in the far-field m-expansion is given by the m-asymptote, $w = \beta_0 \ell_m^{1/3} x^{2/3}$ and $p/E' = \delta_0 \ell_m^{1/3} x^{-1/3}$ (table 1). Let us introduce the normalized opening and pressure

$$\bar{w}(x) = \frac{w(x)}{\ell_m^{1/3} x^{2/3}}, \quad \bar{p}(x) = \frac{1}{E'} \frac{p(x)}{\ell_m^{1/3} x^{-1/3}}. \tag{C 1}$$

Then, the lubrication equation (B 1) can be expressed as

$$x \frac{\mathrm{d}\bar{p}}{\mathrm{d}x} - \frac{\bar{p}}{3} = \frac{1}{\bar{w}^2} + \left(\frac{\ell_{m\tilde{m}}}{x} \right)^{1/6} \frac{1}{\bar{w}^3}, \tag{C 2}$$

https://doi.org/10.1017/S0022112010000501X Published online by Cambridge University Press

where the two terms on the right-hand side correspond to the fluid storage and leak-off, respectively, and $\ell_{m\tilde{m}} = \ell_{\tilde{m}}^9/\ell_m^8$ is the corresponding transitional length scale. An expansion of the solution will be sought as a sum of individual terms from the class of monomial solutions (3.1) of the elasticity equation. Thus, it suffices here to express the monomial solution (3.1) in terms of the normalized quantities (C 1),

$$\bar{w}_\lambda(x) = \frac{B}{x^\lambda}, \quad \bar{p}_\lambda(x) = \frac{Bf\left(\dfrac{2}{3}-\lambda\right)}{x^\lambda}, \quad \text{with } 0 < \frac{2}{3} - \lambda < 1, \tag{C 3}$$

where the function f is defined in (3.1).

Given the presence of the small parameter $(\ell_{m\tilde{m}}/x)^{1/6}$ in the lubrication equation (C 2), an expansion of $\bar{w}(x)$ and $\bar{p}(x)$ can be sought as Taylor series in this parameter, as long as each Taylor term in the expansion corresponds to a valid monomial elastic solution (C 3). Specifically, we write

$$x \to \infty: \quad \left.\begin{aligned} \bar{w} &= \sum_{j=0}^{3} \beta_{-j} \left(\frac{\ell_{m\tilde{m}}}{x}\right)^{j/6} + (\beta_{-4})_* \left(\frac{\ell_{m*}}{x}\right)^{2/3-h} \\ \bar{p} &= \sum_{j=0}^{3} \beta_{-j}\, f\left(\frac{2}{3}-\frac{j}{6}\right) \left(\frac{\ell_{m\tilde{m}}}{x}\right)^{j/6} + (\beta_{-4})_*\, f(h) \left(\frac{\ell_{m*}}{x}\right)^{2/3-h} \end{aligned}\right\}. \tag{C 4}$$

The Taylor terms (under the sum sign in (C 4)) are limited to the highest-order term $O(x^{-1/2})$ corresponding to $j = 3$, which satisfies the exponent constraint in (C 3). Instead, an $O(x^{-2/3+h})$ term is inserted in (C 4) to represent potential non-Taylor term(s) of the sought expansions.

Coefficients β_{-j} of the four Taylor terms ($j = 0, 1, 2, 3$) are obtained using the straightforward matching of the $O(x^{-j/6})$ terms in (C 2) with (C 4), with the result recorded in (3.11). This leads to the following asymptotic form of (C 2) once lower-order terms have been eliminated:

$$x \to \infty: \quad -(1-h)\,(\beta_{-4})_*\; f\,(h)\; x^{-2/3+h} = -\frac{2}{\beta_0^3}\,(\beta_{-4})_*\; x^{-2/3+h} + O(x^{-2/3}), \tag{C 5}$$

where $O(x^{-2/3})$ is the leading order of the second term on the right-hand side of (C 2). By allowing $h > 0$, matching of leading $O(x^{-2/3+h})$ terms in (C 5) results in a transcendental equation on h,

$$(1-h)\; f\,(h) = 2/\beta_0^3, \tag{C 6}$$

which was previously obtained in connection with the similar asymptotic considerations for the zero-leak-off case (Garagash & Detournay 2005). Numerical solution of (C 6), $h \simeq 0.138673$, validates the *a priori* assumption of a positive h, and effectively confirms the existence of the non-Taylor term in the expansions (C 4). The corresponding coefficient $(\beta_{-4})_*$ and the length scale ℓ_{m*} are undetermined from this asymptotic analysis. The expressions of the final expansions, as follows from (C 4) with (C 1), are shown in (3.10*a*, *b*).

Appendix D. Intermediate-field $\widetilde{m}$-expansion (3.13*a*, *b*)

As stipulated in § 3.4, the intermediate leak-off–viscosity $\widetilde{m}$-asymptote, $w = \tilde{\beta}_0\, \ell_{\tilde{m}}^{3/8}\, x^{5/8}$ and $p/E' = \tilde{\delta}_0\, \ell_{\tilde{m}}^{3/8}\, x^{-3/8}$ (table 1), emerge in the intermediate range of distances from the tip $\ell_{\tilde{m}k} \ll x \ll \ell_{m\tilde{m}}$, when the two pertinent transitional length scales

https://doi.org/10.1017/S002211201000501X Published online by Cambridge University Press

separate, i.e. $\ell_{\tilde{m}k} \ll \ell_{m\tilde{m}}$ or $\chi \gg 1$ (3.5). The intermediate-field expansion quantifies the toughness and storage corrections to the $\widetilde{m}$-asymptote as the position x is pulled outside the above intermediate region in the direction towards the tip and the tail of the semi-infinite crack, respectively. In the following, we first quantify these corrections independently of each other in the zero-storage case ($\ell_{m\tilde{m}} = \infty$) and the zero-toughness case ($\ell_{\tilde{m}k} = 0$), respectively. Then, we show that these corrections can be combined into the single expansion (3.13a, b) valid at the intermediate range of distances from the tip in the large χ solution.

Heeding the above, let us introduce normalized opening and pressure as follows:

$$\bar{w}(x) = \frac{w(x)}{\ell_{\tilde{m}}^{3/8}\, x^{5/8}}, \quad \bar{p}(x) = \frac{1}{E'}\frac{p(x)}{\ell_{\tilde{m}}^{3/8}\, x^{-3/8}}. \tag{D 1}$$

Then, the lubrication equation (B 1) can be expressed as

$$x\frac{\mathrm{d}\bar{p}}{\mathrm{d}x} - \frac{3\bar{p}}{8} = \left(\frac{x}{\ell_{m\tilde{m}}}\right)^{1/8}\frac{1}{\bar{w}^2} + \frac{1}{\bar{w}^3}, \tag{D 2}$$

where the two terms on the right-hand side correspond to fluid storage and leak-off, respectively. The class of monomial solutions (3.1) of the elasticity equation can be expressed in terms of normalized quantities (D 1) as

$$\bar{w}_\lambda(x) = B\, x^\lambda, \quad \bar{p}_\lambda(x) = B\ f\left(\tfrac{5}{8}+\lambda\right) x^\lambda, \quad \text{with } 0 < \tfrac{5}{8}+\lambda < 1. \tag{D 3}$$

D.1. *Toughness correction term in the $\widetilde{m}$-expansion under zero-storage conditions ($\ell_{m\tilde{m}} = \infty$)*

In this case, the far-field ($x \gg \ell_{\tilde{m}k}$) expansion of the $\widetilde{m}k$-edge solution is sought. The storage term in the lubrication equation (D 2) is zero, resulting in the reduced equation

$$x\frac{\mathrm{d}\bar{p}}{\mathrm{d}x} - \frac{3\bar{p}}{8} = \frac{1}{\bar{w}^3}. \tag{D 4}$$

Since there is no small parameter in (D 4) to suggest any Taylor terms in the sought $x \to \infty$ expansion, we seek the latter as the sum of the leading ($\widetilde{m}$-asymptote) and next-order toughness correction term of the form (D 3),

$$x \to \infty: \quad \bar{w} = \tilde{\beta}_0 + \tilde{\beta}_{-1}\left(\frac{\ell_{\tilde{m}k}}{x}\right)^{5/8-\tilde{h}}, \quad \bar{p} = \tilde{\beta}_0\, f(5/8) + \tilde{\beta}_{-1}\, f(\tilde{h})\left(\frac{\ell_{\tilde{m}k}}{x}\right)^{5/8-\tilde{h}}. \tag{D 5}$$

Evaluating terms in lubrication equation (D 4) to the $O(x^{-5/8+\tilde{h}})$ terms leads to

$$x \to \infty: \quad -(1-h)\,\tilde{\beta}_{-1}\, f(\tilde{h})\, x^{-5/8+\tilde{h}} = -\frac{3}{\tilde{\beta}_0^4}\,\tilde{\beta}_{-1}\, x^{-5/8+\tilde{h}}. \tag{D 6}$$

The latter yields a transcendental equation in $\tilde{h}$, whose numerical solution is $\tilde{h} \approx 0.06999$. The coefficient $\tilde{\beta}_{-1}$ in (D 5) is undetermined from the asymptotic analysis.

D.2. *Storage correction terms in the $\widetilde{m}$-expansion under zero-toughness conditions ($\ell_{\tilde{m}k} = 0$)*

In this case, the near-field ($x \ll \ell_{m\tilde{m}}$) expansion of the $\widetilde{m}m$-edge solution is sought. The form of lubrication equation (D 2) suggests a Taylor series expansion of the solution

https://doi.org/10.1017/S0022112010005O1X Published online by Cambridge University Press

in the small parameter $(x/\ell_{m\tilde{m}})^{1/8}$,

$$x \to 0: \quad \bar{w} = \sum_{j=0}^{2} \tilde{\beta}_j \left(\frac{x}{\ell_{m\tilde{m}}}\right)^{j/8}, \quad \bar{p} = \sum_{j=0}^{2} \tilde{\beta}_j \; f\left(\frac{5}{8}+\frac{j}{8}\right) \left(\frac{x}{\ell_{m\tilde{m}}}\right)^{j/8}, \tag{D 7}$$

whose terms are of the monomial form (D 3) satisfying the elasticity equation. Only terms with $j \leqslant 2$ are used in (D 7) to abide by the elastic constraint $(5/8)+(j/8)<1$ (D 3). The coefficients $\tilde{\beta}_j$ are established by matching the $O(x^{j/8})$ terms in (D 2) with (D 7), resulting in explicit but lengthy expressions whose numerical evaluations are shown in (3.14). We further note that the Taylor series (D 7) can be extended by the term with $j=3$, when we recognize that although $(5/8)+(j/8)=1$ in this case and the monomial solution (D 3) is not a valid solution of the elasticity equation over the entire semi-infinite crack, it still constitutes a valid $x \to 0$ asymptote of the latter,

$$x \to 0: \quad \bar{w}_{3/8}(x) = B\, x^{3/8}, \quad \bar{p}_{3/8}(x) = \frac{B}{4\pi}\, x^{3/8} \ln x, \tag{D 8}$$

where B is an arbitrary coefficient. (Refer to Appendix B for the proof of considerations for the logarithmic and linear terms in the k-expansions for the pressure and opening, respectively, identical to (D 8) in view of (D 1).) Thus, the terms $\tilde{\beta}_3\,(x/\ell_{m\tilde{m}})^{3/8}$ and $(\tilde{\beta}_3/4\pi)\,(x/\ell_{m\tilde{m}})^{3/8}\ln x$ can be added to the expansions for the opening and the net pressure in (D 7), respectively, with the value of the coefficient $\tilde{\beta}_3$ obtained from the matching of the terms of $O(x^{3/8})$ in (D 2).

The possible existence of a non-Taylor term $O(x^h)$, with $h>0$, in the near-field expansion is excluded, as a direct evaluation of the corresponding $O(x^h)$ terms in the lubrication equation (D 2) yields

$$x \to 0: \left(h-\frac{3}{8}\right) \; f\left(\frac{5}{8}+h\right) \; x^h = -\frac{3}{\tilde{\alpha}_0^4}\, x^h. \tag{D 9}$$

Indeed, the computed exponent, $h \simeq 0.9698$, violates the elastic constraint $(5/8)+h<1$.

D.3. *The $\widetilde{m}$-expansion*

In the following, we show that in the general case, the $\widetilde{m}$-expansion is given by a combination of the two limit expansions obtained above.

Let us consider the large χ solution in the coordinate range $x \ll \ell_{m\tilde{m}}$. The $O(1)$ solution in that coordinate range is given by the zero-storage $\widetilde{m}k$-edge solution, while the next-order solution corresponds to a small storage $\chi^{-1} = (\ell_{\tilde{m}k}/\ell_{m\tilde{m}})^{1/8} \ll 1$ perturbation. This is evident when the lubrication equation (D 2) is rewritten using the appropriately scaled coordinate $\xi = x/\ell_{\tilde{m}k}$,

$$\xi \frac{\mathrm{d}\bar{p}}{\mathrm{d}\xi} - \frac{3\bar{p}}{8} = \chi^{-1} \frac{\xi^{1/8}}{\bar{w}^2} + \frac{1}{\bar{w}^3}, \quad \left(\xi = \frac{x}{\ell_{\tilde{m}k}}\right), \tag{D 10}$$

with the first term on the right-hand side corresponding to a small storage correction at distances from the tip $\xi \ll \chi^{-8}$ $(x \ll \ell_{m\tilde{m}})$. Therefore, the next-order large χ solution for $x \ll \ell_{m\tilde{m}}$ can be sought as a Taylor expansion in the small storage parameter $\chi^{-1} \ll 1$,

$$\bar{w} = \bar{w}^{(0)} + \chi^{-1}\, \bar{w}^{(1)} + \cdots, \quad \bar{p} = \bar{p}^{(0)} + \chi^{-1}\, \bar{p}^{(1)} + \cdots, \tag{D 11}$$

with the $O(1)$ term, $\{\bar{w}^{(0)},\ \bar{p}^{(0)}\}$, given by the zero-storage $\widetilde{m}k$-edge solution. The equations for the $O(\chi^{-1})$ term follow from the requisite expansions of the lubrication

https://doi.org/10.1017/S002211201000501X Published online by Cambridge University Press

(D 10) and elasticity (2.3):

$$O(\chi^{-1}): \quad \xi\frac{\mathrm{d}\bar{p}^{(1)}}{\mathrm{d}\xi}-\frac{3\bar{p}^{(1)}}{8}=\frac{\xi^{1/8}}{(\bar{w}^{(0)})^2}-\frac{\bar{w}^{(1)}}{(\bar{w}^{(0)})^4}, \quad \bar{p}^{(1)}=\mathscr{L}[\bar{w}^{(1)}]. \qquad \text{(D 12}a,\,b\text{)}$$

The far-field ($\ell_{\tilde{m}k}\ll x$) asymptotics of the $O(1)$ term $\{\bar{w}^{(0)},\,\bar{p}^{(0)}\}$ is given by (D 5). In view of that, and assuming a monomial form (D 3) for the far-field asymptote of $\{\bar{w}^{(1)},\,\bar{p}^{(1)}\}$, the latter is found from balancing terms in (D.12a) in the form $\bar{w}^{(1)}=\tilde{\beta}_1\,\xi^{1/8}$ and $\bar{p}^{(1)}=\tilde{\beta}_1\,f\,(3/4)\,\xi^{1/8}$. (The value of $\tilde{\beta}_1$ is given in (3.14).) Consequently, using (D 11), the far-field expansion of the large χ solution in the coordinate range $x\ll\ell_{m\tilde{m}}$ is given by

$$\left.\begin{aligned}\xi=\frac{x}{\ell_{\tilde{m}k}}\gg 1: \quad \bar{w}&=\tilde{\beta}_0+\frac{\tilde{\beta}_{-1}}{\xi^{5/8-\tilde{h}}}+\chi^{-1}\,\tilde{\beta}_1\,\xi^{1/8},\\ \bar{p}&=\tilde{\beta}_0\,f\left(\frac{5}{8}\right)+\frac{\tilde{\beta}_{-1}\,f\,(\tilde{h})}{\xi^{5/8-\tilde{h}}}+\chi^{-1}\,\tilde{\beta}_1\,f\left(\frac{3}{4}\right)\xi^{1/8}.\end{aligned}\right\} \qquad \text{(D 13)}$$

We observe that the asymptotic expression (D 13) is a combination of the $\widetilde{m}k$-edge far-field expansion (D 5), with the first next-order term in the $m\widetilde{m}$-edge near-field expansion (D 7).

Repeating this analysis for higher order, $O(\chi^{-2})$ and $O(\chi^{-3})$, storage corrections added to (D 11) would lead to an enrichment of the far-field ($\ell_{\tilde{m}k}\ll x$) expansion (D 13), with the remaining next-order terms from the $m\widetilde{m}$-edge expansion. This effectively proves that the expansion of the large χ solution in the intermediate range ($\ell_{\tilde{m}k}\ll x\ll\ell_{m\tilde{m}}$) of distances from the tip is given by the combination (3.13a, b) of the $\widetilde{m}k$-edge far-field and the $m\widetilde{m}$-edge near-field expansions.

We note here (leaving out the actual proof) that the same conclusion can be reached by considering the large χ solution in the coordinate range $x\gg\ell_{\tilde{m}k}$. In this case, the $O(1)$ solution is given by the zero-toughness $m\widetilde{m}$-edge solution, while the next-order solution in that coordinate range corresponds to a small toughness χ^{-1} perturbation. The details of the treatment are similar to these given above, with the important distinction being that the actual form of the toughness (χ^{-1}) dependence of the next-order large χ solution in the range $x\gg\ell_{\tilde{m}k}$ is not intrinsic to that solution. Instead, it is determined from the matching of this solution with the large χ solution in the range $x\ll\ell_{m\tilde{m}}$ (discussed above) in the overlapping coordinate range $\ell_{\tilde{m}k}\ll x\ll\ell_{m\tilde{m}}$, where both solutions are thought to possess the common $\widetilde{m}$-expansion.

Appendix E. Normalized form of asymptotic expansions

The near (3.8), far (3.10a, b) and intermediate (3.13a, b) asymptotic expansions are expressed below in normalized forms utilizing relevant scaling(s), (4.1) and table 2, as indicated.

Near-field k-expansion:

$$mk\text{-scaling},\ \xi\to 0: \quad \begin{aligned}\Omega&=\xi^{1/2}\left[1+4\pi\,(1+\chi)\,\xi^{1/2}+64\,(1+\chi)\left(\frac{2}{3}+\chi\right)\xi\ln\xi\right]\\ \Pi&=(1+\chi)\left[\ln\left[\xi/\xi^{o}(\chi)\right]-24\pi\left(\frac{2}{3}+\chi\right)\xi^{1/2}\right.\\ &\qquad\left.-192\left(\frac{2}{3}+\chi\right)^2\xi\ln\xi\right],\end{aligned} \qquad \text{(E 1}a,\,b\text{)}$$

https://doi.org/10.1017/S0022112010005O1X Published online by Cambridge University Press

$$\widetilde{m}k\text{-scaling, } \xi \to 0: \quad \Omega = \xi^{1/2}\left[1 + 4\pi\left(\frac{1}{\chi}+1\right)\xi^{1/2} + 64\left(\frac{1}{\chi}+1\right) \times \left(\frac{2}{3\chi}+1\right)\xi \ln \xi\right]$$

$$\Pi = \left(\frac{1}{\chi}+1\right)\left[\ln\left[\xi/\xi^{o}(\chi)\right] - 24\pi\left(\frac{2}{3\chi}+1\right)\xi^{1/2} - 192\left(\frac{2}{3\chi}+1\right)^{2}\xi \ln \xi\right]. \tag{E 2a, b}$$

Far-field m-expansion:

$$mk\text{-scaling, } \xi \to \infty: \quad \Omega = \sum_{j=0}^{3} \beta_{-j}\,\chi^{j}\,\xi^{(2/3)-(j/6)} + (\beta_{-4})_{k}(\chi)\,\xi^{h},$$

$$\Pi = \sum_{j=0}^{3} \delta_{-j}\,\chi^{j}\,\xi^{-(1/3)-(j/6)} + (\delta_{-4})_{k}(\chi)\,\xi^{h-1}, \tag{E 3a, b}$$

$$m\widetilde{m}\text{-scaling, } \xi \to \infty: \quad \Omega = \sum_{j=0}^{3} \beta_{-j}\,\xi^{(2/3)-(j/6)} + (\beta_{-4})_{\widetilde{m}}(\chi)\,\xi^{h},$$

$$\Pi = \sum_{j=0}^{3} \delta_{-j}\,\xi^{-(1/3)-(j/6)} + (\delta_{-4})_{\widetilde{m}}(\chi)\,\xi^{h-1}. \tag{E 4a, b}$$

Intermediate-field $\widetilde{m}$-expansion ($\chi \gg 1$):

$$\widetilde{m}k\text{-scaling, } 1 \ll \xi \ll \chi^{8}: \quad \Omega = \tilde{\beta}_{-1}\,\xi^{\tilde{h}} + \sum_{j=0}^{3} \frac{\tilde{\beta}_{j}}{\chi^{j}}\,\xi^{(5+j)/8},$$

$$\Pi = \tilde{\delta}_{-1}\xi^{\tilde{h}-1} + \sum_{j=0}^{2} \frac{\tilde{\delta}_{j}}{\chi^{j}}\xi^{(-3+j)/8} + \frac{\tilde{\delta}_{3}}{\chi^{3}}\ln(\xi/\tilde{\xi}^{o}), \tag{E 5a, b}$$

$$m\widetilde{m}\text{-scaling, } \chi^{-8} \ll \xi \ll 1: \quad \Omega = \chi^{-5+8\tilde{h}}\,\tilde{\beta}_{-1}\,\xi^{\tilde{h}} + \sum_{j=0}^{3} \tilde{\beta}_{j}\,\xi^{(5+j)/8},$$

$$\Pi = \chi^{-5+8\tilde{h}}\,\tilde{\delta}_{-1}\xi^{\tilde{h}-1} + \sum_{j=0}^{2} \tilde{\delta}_{j}\xi^{(-3+j)/8} + \tilde{\delta}_{3}\ln(\xi/\tilde{\xi}^{o}). \tag{E 6a, b}$$

Appendix F. Numerical scheme

In this Appendix, we first present a general numerical approach to compute solution in both limiting (edge solutions) and general cases. The approach is a direct extension of the method used by Garagash & Detournay (2005) for the zero-leak-off case (mk-edge solution) and their earlier work (Garagash & Detournay 2000).

https://doi.org/10.1017/S0022112010005001X Published online by Cambridge University Press

Let us assume that the normalized solution for the net pressure in one of the scalings from table 2 is given with appropriate degree of accuracy by $\Pi_0^*(\xi)$ for $\xi < \Xi_0$ and by $\Pi_\infty^*(\xi)$ for $\xi > \Xi_\infty$. Here $\xi \in (\Xi_0, \Xi_\infty)$ is the normalized computational interval $x \in (X_0, X_\infty)$, and $\Pi_0^*(\xi)$ and $\Pi_\infty^*(\xi)$ designate the relevant near- and far-field asymptotic expansions, respectively, truncated to one or two leading terms where further indicated. Upon discretization of the interval $\xi \in (\Xi_0, \Xi_\infty)$ into $n-1$ subintervals (ξ_i, ξ_{i+1}), $i = 1, \ldots, n-1$ with $\xi_1 = \Xi_0$ and $\xi_n = \Xi_\infty$, the variation of the net pressure over a subinterval is approximated by a linear combination of the leading near-field, $\Pi_0(\xi)$, and far-field, $\Pi_\infty(\xi)$, asymptotes. Thus,

$$\Pi(\xi) = \begin{cases} \Pi_0^*(\xi), & \xi \in (0, \xi_1), \\ a_i\,\Pi_0(\xi) + b_i\,\Pi_\infty(\xi), & \xi \in (\xi_i, \xi_{i+1}), \quad i = 1, \ldots n-1, \\ \Pi_\infty^*(\xi), & \xi \in (\xi_n, \infty). \end{cases} \tag{F 1}$$

Imposing continuity of this approximation at internal nodes, ξ_i $(i = 2, \ldots, n-1)$, allows evaluation of the coefficients in (F 1) in terms of values of the pressure at interval endpoints, $\Pi_i = \Pi(\xi_i)$,

$$a_i = \frac{\Pi_\infty(\xi_i)\,\Pi_{i+1} - \Pi_\infty(\xi_{i+1})\,\Pi_i}{\Pi_\infty(\xi_i)\,\Pi_0(\xi_{i+1}) - \Pi_\infty(\xi_{i+1})\,\Pi_0(\xi_i)}, \quad b_i = -\frac{\Pi_0(\xi_i)\,\Pi_{i+1} - \Pi_0(\xi_{i+1})\,\Pi_i}{\Pi_\infty(\xi_i)\,\Pi_0(\xi_{i+1}) - \Pi_\infty(\xi_{i+1})\,\Pi_0(\xi_i)}. \tag{F 2a}$$

The pressure continuity condition at the computational interval endpoints, ξ_1 and ξ_n, requires

$$\Pi_1 = \Pi_0^*(\xi_1), \quad \Pi_n = \Pi_\infty^*(\xi_n). \tag{F 3}$$

The corresponding approximation to the normalized opening can be evaluated by substituting (F 1) into the normalized version of the elasticity integral (2.4),

$$\Omega(\xi) = \kappa\,\xi^{1/2} + \mathscr{L}^{-1}[\Pi](\xi), \tag{F 4}$$

where the value of the normalized toughness parameter κ depends on the scaling: it is 1 in either the mk- or $\widetilde{m}k$-scalings, and χ^{-1} in the $m\widetilde{m}$-scaling (see the normalized propagation condition in table 2). In the following, we make use of two generalized integral operators, $\mathscr{F}$ and $\mathscr{H}$ (with $\mathscr{F}$ originally introduced in (B 3)),

$$\mathscr{F}\,[\Pi]\,(\xi, \eta) = \frac{4}{\pi}\int_0^\eta K(\xi, \eta)\,\Pi(\eta)\,\mathrm{d}\eta, \quad \mathscr{H}\,[\Pi]\,(\xi, \eta) = \frac{4}{\pi}\int_\eta^\infty K(\xi, \eta)\,\Pi(\eta)\,\mathrm{d}\eta, \tag{F 5}$$

such that both operators reduce to $\mathscr{L}^{-1}[\Pi](\xi)$ when $\eta = \infty$ and $\eta = 0$, respectively. In view of (F 1), the expression (F 4) for the normalized opening then becomes

$$\Omega(\xi) = \kappa\,\xi^{1/2} + \left\{ \mathscr{F}[\Pi_0^*](\xi, \xi_1) + \sum_{i=1}^{n-1} [a_i\,\mathscr{F}[\Pi_0](\xi, \eta) + b_i\,\mathscr{H}[\Pi_\infty](\xi, \eta)]_{\eta=\xi_i}^{\eta=\xi_{i+1}} + \mathscr{H}[\Pi_\infty^*](\xi, \xi_n) \right\}. \tag{F 6}$$

Since functions $\Pi_0(\xi)$ and $\Pi_\infty(\xi)$ correspond to the leading, non-zero terms in functions $\Pi_0^*(\xi)$ and $\Pi_\infty^*(\xi)$, respectively, we further discuss evaluation of $\mathscr{F}[\Pi_0^*](\xi, \eta)$ and $\mathscr{H}[\Pi_\infty^*](\xi, \eta)$ only.

For the general solution $(0 < \chi < \infty)$ in the mk-scaling, the function $\Pi_0^*(\xi)$ is given by the (possibly truncated) asymptotic expansion (E 1b), and $\mathscr{F}[\Pi_0^*](\xi, \eta)$

https://doi.org/10.1017/S002211201000501X Published online by Cambridge University Press

can be evaluated as a linear combination of functions $\mathscr{F}[\ln\eta](\xi,\eta)$, $\mathscr{F}[1](\xi,\eta)$, $\mathscr{F}[\eta^{1/2}](\xi,\eta)$ and $\mathscr{F}[\eta\ln\eta](\xi,\eta)$, which are given by expressions (C 17)–(C 20) of Garagash & Detournay (2005), respectively, multiplied by $4/\pi$. On the other hand, the function $\Pi^*_\infty(\xi)$ is given by the (possibly truncated) asymptotic expansion (E 3*b*), and consequently $\mathscr{H}[\Pi^*_\infty](\xi,\eta)$ can be evaluated as a linear combination of functions $\mathscr{H}[\eta^{h-1}](\xi,\eta)$ with appropriate set of values $h\in(0,1)$. The latter function was provided by Garagash & Detournay (2005): see their (C 21) multiplied by $4/\pi$.

Considering the mk-, $\widetilde{m}k$- and $m\widetilde{m}$-edge solutions, the function $\Pi^*_0(\xi)$ is defined by the asymptotic expansion (E 1*b*) with $\chi=0$, (E 2*b*) with $\chi\to\infty$, and (E 6*b*) with $\chi\to\infty$, respectively. Consequently, for the mk- and $\widetilde{m}k$-edge, $\mathscr{F}[\Pi^*_0](\xi,\eta)$ is a linear combination of the same set of functions as for the general solution discussed above. For the $m\widetilde{m}$-edge, $\mathscr{F}[\Pi^*_0](\xi,\eta)$ is a linear combination of functions $\mathscr{F}[\eta^{h-1}](\xi,\eta)=\pi h^{-1}\tan\pi h\,\xi^h-\mathscr{H}[\eta^{h-1}](\xi,\eta)$ with an appropriate set of values $h\in(0,1)$, as well as of functions $\mathscr{F}[\ln\eta](\xi,\eta)$ and $\mathscr{F}[1](\xi,\eta)$. On the other hand, $\Pi^*_\infty(\xi)$ for the above three edge solutions in their respective scalings is defined by asymptotic expansion (E 3*b*) with $\chi=0$, (E 5*b*) with $\chi\to\infty$ and (E 4*b*) with $\chi\to\infty$, respectively. A survey of terms in the expansions mentioned yields that $\mathscr{H}[\Pi^*_\infty](\xi,\eta)$ in each of the edge solutions can be evaluated as an appropriate linear combination of functions $\mathscr{H}[\eta^{h-1}](\xi,\eta)$ with $h\in(0,1)$.

Using these approximations for the net pressure (F 1) and opening (F 6), evaluation of the appropriately normalized lubrication equation (table 2) at n subintervals' midpoints, $\xi_{i+1/2}=0.5\,(\xi_i+\xi_{i+1})$, together with (F 3) yields a system of $n+2$ nonlinear algebraic equations. Its unknowns are the values of the net pressure at $n+1$ grid points and additional unknown coefficients in the near-field $\Pi^*_0(\xi)$ and far-field $\Pi^*_\infty(\xi)$ expansions (or truncated parts thereof). Two possibilities with respect to the choice of Π^*_0 and Π^*_∞ are considered below.

(i) When the complete near- and far-field asymptotic expansions (Appendix E), each containing one unknown coefficient, are used, the system of $n+2$ equations as formulated above is insufficient to solve for the $n+3$ unknowns and an additional constraint needs to be introduced. This is chosen in the form

$$\Pi_{n-1}=\Pi^*_\infty(\xi_{n-1}). \tag{F 7}$$

An alternative constraint corresponding to the evaluation of the lubrication equation just outside the originally set computation interval can be used with the same success (Garagash & Detournay 2005).

(ii) Near- and/or far-field expansions are truncated in such a way that only one unknown coefficient is left between them. In this case, the originally formulated system of $n+2$ equations is complete.

The first option is used to compute all three edge solutions, whereas the second option is used to compute the general solution with $0<\chi<\infty$. Specifically for the general solution in the mk-scaling, with $\Pi_0(\xi)=(1+\chi)\ln\xi$ and $\Pi_\infty(\xi)=\delta_0\xi^{-1/3}$, the following two- and one-term truncations were used in the near and far field: $\Pi^*_0(\xi)=(1+\chi)\,(\ln\xi-\ln\xi^o(\chi))$ and $\Pi^*_\infty(\xi)=\delta_0\xi^{-1/3}$, respectively. The truncation was dictated by the existence of a numerical instability that appears for large values of χ when all the terms in the expansions are used. Use of fewer expansion terms in the near and far fields of the numerical solution also required a wider than otherwise warranted computational interval to ensure convergence of the solution towards the set near- and far-field behaviours.

The computational intervals utilized for the three edge solutions and the general solution are listed in table 6. These intervals were discretized into $n=100$ of a

https://doi.org/10.1017/S002211201000501X Published online by Cambridge University Press

Solution	Bounds of computational intervals	
mk-edge ($\chi = 0$)	$X_0 = 10^{-6}\,\ell_{mk}$	$X_\infty = 10^{2}\,\ell_{mk}$
$\tilde{m}k$-edge ($\chi \to \infty$)	$X_0 = 10^{-7}\,\ell_{\tilde{m}k}$	$\widetilde{X}_\infty = 10^{2}\,\ell_{\tilde{m}k}$
$m\tilde{m}$-edge ($\chi \to \infty$)	$\widetilde{X}_0 = 10^{-4}\,\ell_{m\tilde{m}}$	$X_\infty = 10^{3}\,\ell_{m\tilde{m}}$
General ($0 < \chi < \infty$)	$X_0 = 10^{-7}\begin{cases}\ell_{mk}, & \chi < 1\\ \ell_{\tilde{m}k}, & \chi \geqslant 1\end{cases}$	$X_\infty = 10^{4}\begin{cases}\ell_{mk}, & \chi < 1\\ \ell_{m\tilde{m}}, & \chi \geqslant 1\end{cases}$

TABLE 6. Computational bounds.

uniform logarithmic measure for the edge solutions and into $n = 160$ subintervals for the general solution. The corresponding systems of nonlinear algebraic equations, as formulated above, were solved using the built-in Newtonian iteration procedure in *Mathematica*, Ver. 6 (Wolfram Research, Inc., 1988–2007).

REFERENCES

ABÉ, H., MURA, T. & KEER, L. M. 1976 Growth rate of a penny-shaped crack in hydraulic fracturing of rocks. *J. Geophys. Res.* **81**, 5335–5340.

ADACHI, J. I. & DETOURNAY, E. 2002 Self-similar solution of a plane-strain fracture driven by a power-law fluid. *Intl J. Numer. Anal. Meth. Geomech.* **26**, 579–604.

ADACHI, J. I. & DETOURNAY, E. 2008 Plane-strain propagation of a hydraulic fracture in a permeable rock. *Engng Fract. Mech.* **75**, 4666–4694.

ADVANI, S. H., TOROK, J. S., LEE, J. K. & CHOUDHRY, S. 1987 Explicit time-dependent solutions and numerical evaluations for penny-shaped hydraulic fracture models. *J. Geophys. Res.* **92** (B8), 8049–8055.

BARENBLATT, G. I. 1956 On the formation of horizontal cracks in hydraulic fracture of an oil-bearing stratum. *Prikl. Mat. Mech.* **20**, 475–486.

BATCHELOR, G. K. 1967 *An Introduction to Fluid Dynamics*. Cambridge University Press.

BILBY, B. & ESHELBY, J. 1968 Dislocations and the theory of fracture. In *Fracture, an Advanced Treatise* (ed. H. Liebowitz), vol. I, chapter 2, pp. 99–182. Academic.

BUNGER, A. P. & DETOURNAY, E. 2007 Early time solution for a penny-shaped hydraulic fracture. *ASCE J. Engng Mech.* **133** (5), 534–540.

BUNGER, A. P. & DETOURNAY, E. 2008 Experimental validation of the tip asymptotics for a fluid-driven crack. *J. Mech. Phys. Solids* **56**, 3101–3115.

BUNGER, A. P., DETOURNAY, E. & GARAGASH, D. I. 2005 Toughness-dominated hydraulic fracture with leak-off. *Intl J. Fract.* **134**, 175–190.

CARBONELL, R., DESROCHES, J. & DETOURNAY, E. 1999 A comparison between a semi-analytical and a numerical solution of a two-dimensional hydraulic fracture. *Intl J. Solids Struct.* **36** (31–32), 4869–4888.

CARTER, E. 1957 Optimum fluid characteristics for fracture extension. In *Drilling and Production Practices* (ed. G. Howard & C. Fast), pp. 261–270. American Petroleum Institute.

DESROCHES, J., DETOURNAY, E., LENOACH, B., PAPANASTASIOU, P., PEARSON, J. R. A., THIERCELIN, M. & CHENG, A. H.-D. 1994 The crack tip region in hydraulic fracturing. *Proc. R. Soc. Lond.* A **447**, 39–48.

DETOURNAY, E. & GARAGASH, D. 2003 The tip region of a fluid-driven fracture in a permeable elastic solid. *J. Fluid Mech.* **494**, 1–32.

DETOURNAY, E. & GARAGASH, D. I. 2010 General scaling laws for fluid-driven fractures. *Proc. R. Soc. Lond.* A (submitted).

ECONOMIDES, M. J. & NOLTE, K. G. 2000 *Reservoir Stimulation*. Wiley.

EMERMAN, S., TURCOTTE, D. & SPENCE, D. 1986 Transport of magma and hydrothermal solutions by laminar and turbulent fluid fracture. *Phys. Earth Planet. Intl* **36**, 276–284.

GARAGASH, D. I. 2006*a* Plane strain propagation of a fluid-driven fracture during injection and shut-in: asymptotics of large toughness. *Engng Frac. Mech.* **73**, 456–481.

https://doi.org/10.1017/S002211201000501X Published online by Cambridge University Press

Garagash, D. I. 2006*b* Propagation of a plane-strain hydraulic fracture with a fluid lag: early-time solution. *Intl J. Solids Struct.* **43**, 5811–5835.

Garagash, D. I. 2006*c* Transient solution for a plane-strain fracture driven by a shear-thinning, power-law fluid. *Intl J. Numer. Anal. Meth. Geomech.* **30** (14), 1439–1475.

Garagash, D. I. 2009 Scaling of physical processes in fluid-driven fracture: perspective from the tip. In *IUTAM Symposium on Scaling in Solid Mechanics* (ed. F. Borodich), IUTAM Bookseries, vol. 10, pp. 91–100. Springer.

Garagash, D. I. 2010 Plane-strain propagation of a fluid-driven fracture in a permeable medium: leak-off dominated regime. *Intl J. Solids Struct.* (submitted).

Garagash, D. I. & Detournay, E. 2000 The tip region of a fluid-driven fracture in an elastic medium. *ASME J. Appl. Mech.* **67** (1), 183–192.

Garagash, D. I. & Detournay, E. 2005 Plane-strain propagation of a fluid-driven fracture: small toughness solution. *ASME J. Appl. Mech.* **72** (6), 916–928.

Geertsma, J. & Haafkens, R. 1979 A comparison of the theories for predicting width and extent of vertical hydraulically induced fractures. *ASME J. Energy Res. Tech.* **101**, 8–19.

Geertsma, J. & de Klerk, F. 1969 A rapid method of predicting width and extent of hydraulic induced fractures. *J. Petrol. Tech.* **246**, 1571–1581.

Hu, J. & Garagash, D. I. 2010. Plane-strain fluid-driven fracture propagation in a permeable rock of finite toughness. *ASCE J. Eng. Mech.* **136**, 1152–1156.

Irwin, G. R. 1957 Analysis of stresses and strains near the end of a crack traversing a plate. *ASME J. Appl. Mech.* **29**, 361–364.

Kanninen, M. F. & Popelar, C. H. 1985 *Advanced Fracture Mechanics.* The Oxford Engineering Science Series, vol. 15. Oxford University Press.

Khristianovic, S. & Zheltov, Y. 1955 Formation of vertical fractures by means of highly viscous fluids. In *Proceedings of the 4th World Petroleum Congress*, Rome, vol. 2, pp. 579–586. Carlo Colombo Publishers.

Lecampion, B. & Detournay, E. 2007 An implicit algorithm for the propagation of a hydraulic fracture with a fluid lag. *Comput. Meth. Appl. Mech. Engng* **196**, 4863–4880.

Lenoach, B. 1995 The crack tip solution for hydraulic fracturing in a permeable solid. *J. Mech. Phys. Solids* **43** (7), 1025–1043.

Lister, J. R. 1990 Buoyancy-driven fluid fracture: the effects of material toughness and of low-viscosity precursors. *J. Fluid Mech.* **210**, 263–280.

Madyarova, M. & Detournay, E. 2010 Fluid-driven penny-shaped fracture in permeable rock. *Intl J. Numer. Anal. Meth. Geomech.* (submitted).

Mendelsohn, D. A. 1984 A review of hydraulic fracture modeling. Part I. General concepts, 2D models, motivation for 3D modeling. *ASME J. Energy Res. Tech.* **106**, 369–376.

Nordgren, R. 1972 Propagation of vertical hydraulic fractures. *J. Petrol. Tech.* **253**, 306–314.

Peirce, A. P. 2010 A Hermite cubic collocation scheme for plane strain hydraulic fracture problems. *Comput. Meth. Appl. Mech. Engng* **199**, 1949–1962.

Peirce, A. & Detournay, E. 2008 An implicit level set method for modeling hydraulically driven fractures. *Comput. Meth. Appl. Mech. Engng* **197**, 2858–2885.

Perkins, T. K. & Kern, L. R. 1961 Widths of hydraulic fractures. *J. Petrol. Tech.* **222**, 937–949.

Rice, J. R. 1968 Mathematical analysis in the mechanics of fracture. In *Fracture: An Advanced Treatise* (ed. H. Liebowitz), vol. II, chapter 3, pp. 191–311. Academic.

Rubin, A. 1993 Tensile fracture of rock at high confining pressure: implications for dike propagation. *J. Geophys. Res.* **98**, 15919–15935.

Rubin, A. 1995 Propagation of magma-filled cracks. *Annu. Rev. Earth Planet. Sci.* **23**, 287–336.

Savitski, A. & Detournay, E. 2002 Propagation of a fluid-driven penny-shaped fracture in an impermeable rock: asymptotic solutions. *Intl J. Solids Struct.* **39** (26), 6311–6337.

Spence, D., Sharp, P. & Turcotte, D. 1987 Buoyancy-driven crack propagation: a mechanism for magma migration. *J. Fluid Mech.* **174**, 135–153.

Spence, D. & Turcotte, D. 1985 Magma-driven propagation of cracks. *J. Geophys. Res.* **90**, 575–580.

Spence, D. A. & Sharp, P. W. 1985 Self-similar solution for elastohydrodynamic cavity flow. *Proc. R. Soc. Lond.* A **400**, 289–313.

https://doi.org/10.1017/S002211201000501X Published online by Cambridge University Press